Seismic Stratigraphy of Contourite Drift Deposits Associated with the Loop Current on the Eastern Campeche Bank, Gulf of Mexico

Christopher M. Lowery[1]*, Ligia Perez Cruz[2,3], Jaime Urrutia Fucugauchi[2,3], Jingxuan Wei[1], James A. Austin, Jr.[1], Patricia Standring[1]

[1]Institute for Geophysics, Jackson School of Geosciences, University of Texas, Austin, USA

[2]Instituto de Geofísica, Universidad Nacional Autónoma De México, Mexico City, Mexico

[3]Instituto de Investigación y Estudios Avanzados Chicxulub, Merida, Yucatan, Mexico

*corresponding author: cmlowery@utexas.edu

Key Points:

- High resolution multichannel seismic data reveal the evolution of contourite drifts associated with the Loop Current
- Contourite deposition began in the Cenozoic, and overlies early Cenozoic and Late Cretaceous pelagic sediments with little evidence of bottom currents
- Comparison of seismic facies with those present at nearby Deep Sea Drilling Project Site 95 suggest the Loop Current began in the Early Oligocene

Abstract

The Loop Current is a key component of the northward transport of warm, salty water and an important influence on Gulf of Mexico hydrography. Understanding how the Loop Current will respond to ongoing anthropogenic warming is critically important, but the history of the Loop Current is poorly known. Here, we present the results of a high resolution multichannel seismic survey of sediment drifts on the eastern Campeche Bank associated with the Loop Current. We identify three seismic megasequences: Megasequence A is an Early Cretaceous carbonate platform, Megasequence B comprises Cretaceous to early Cenozoic pelagic carbonates with weak/no contourite current flow, and Megasequence C comprises a series of large contourite drifts representing the inception and history of the Loop Current. The base of the contourites is marked by a regionally mappable unconformity eroding underling strata, sometimes incising hundreds of meters. The drifts contain a succession of sequence sets separated from each other by regional unconformities and comprising massive elongated mounded sediment drifts, then plastered drifts, and then back the massive elongated drifts which characterize modern deposition, with active moats forming on the seafloor. A lack of sediment cores in the study area precludes age determination of these drift deposits, with the exception of the youngest (Late Pleistocene). Comparison to legacy seismic lines across Deep Sea Drilling Project Site 95, just outside our study area, implies that the base of Megasequence C is Oligocene, and that the Loop Current developed during the global reorganization of ocean circulation at the Eocene-Oligocene Transition.

Plain Language Summary

The Loop Current flows into the Gulf of Mexico from the Caribbean through the Yucatán Strait, and exits to the Atlantic Ocean through the Straits of Florida. The Loop Current is part of a series of currents that carry warm, salty water to the far North Atlantic, where it cools and sinks, a critical part of global ocean circulation. It is also important for Gulf of Mexico climate, as it sometimes spins off warm eddies which drift west, disrupting fisheries and providing a warm water fuel source for hurricanes. Because it is so important to global and regional climate, it is important to understand how the Loop Current will respond to ongoing climate change, and one essential part of that is seeing how it responded to past climate change. Here, we report the results

of a seismic survey of a sediment drift on the eastern Campeche Bank which records the initiation and history of the Loop Current. A lack of sediment cores in this area make it hard to put age constraints on our observations, so we evaluate several plausible hypotheses about when the Loop Current first formed and what that means for the current's future.

1. Introduction

The Loop Current (Figure 1) is a key component of the global thermohaline circulation and an important driver of regional and global climate. As one of the main feeder currents of the Gulf Stream, the Loop Current is a major part of the western boundary current system in the North Atlantic that moves warm, salty water from the tropics towards the Greenland, Iceland, and Labrador seas, where it cools and sinks to form North Atlantic Deep Water, the main driver of Atlantic Meridional Overturning Circulation (AMOC). The Loop Current also controls the average oceanographic characteristics of surface waters in the Gulf of Mexico by aperiodically spinning off warm-core eddies which drift west (Thirumalai et al., 2021). Eddy shedding is a complex process that remains only partially understood (e.g., Weisberg and Liu, 2017). Individual eddies can disrupt fisheries, strain offshore infrastructure, and provide a potent warm-water fuel source for hurricanes (e.g., Biggs, 1992, Bosart et al., 1999; Milkov and Sassen, 2000). Warming attributed to these eddies is also a possible driver of sea level rise rates in the Gulf of Mexico that exceed the global average (Steinberg et al., 2023).

For these reasons, it is imperative to understand how the Loop Current will respond to anthropogenic warming. The National Academies of Science, Engineering, and Medicine (NASEM) recently published a detailed report cataloguing all the things that we do not know about the Loop Current (NASEM 2019), emphasizing knowledge gaps regarding modern hydrography and eddy formation. This publication was followed by the announcement of a NASEM funding program to address these knowledge gaps using hydrographic observations and modelling. A glaring gap in this important effort is the lack of any perspective on past Loop Current changes. Modern hydrographic observations provide an important mechanistic understanding of the dynamic processes which govern the Loop Current, but only within the narrow climatological framework of the late 20th and early 21st centuries. As atmospheric pCO_2 approaches levels last reached in the

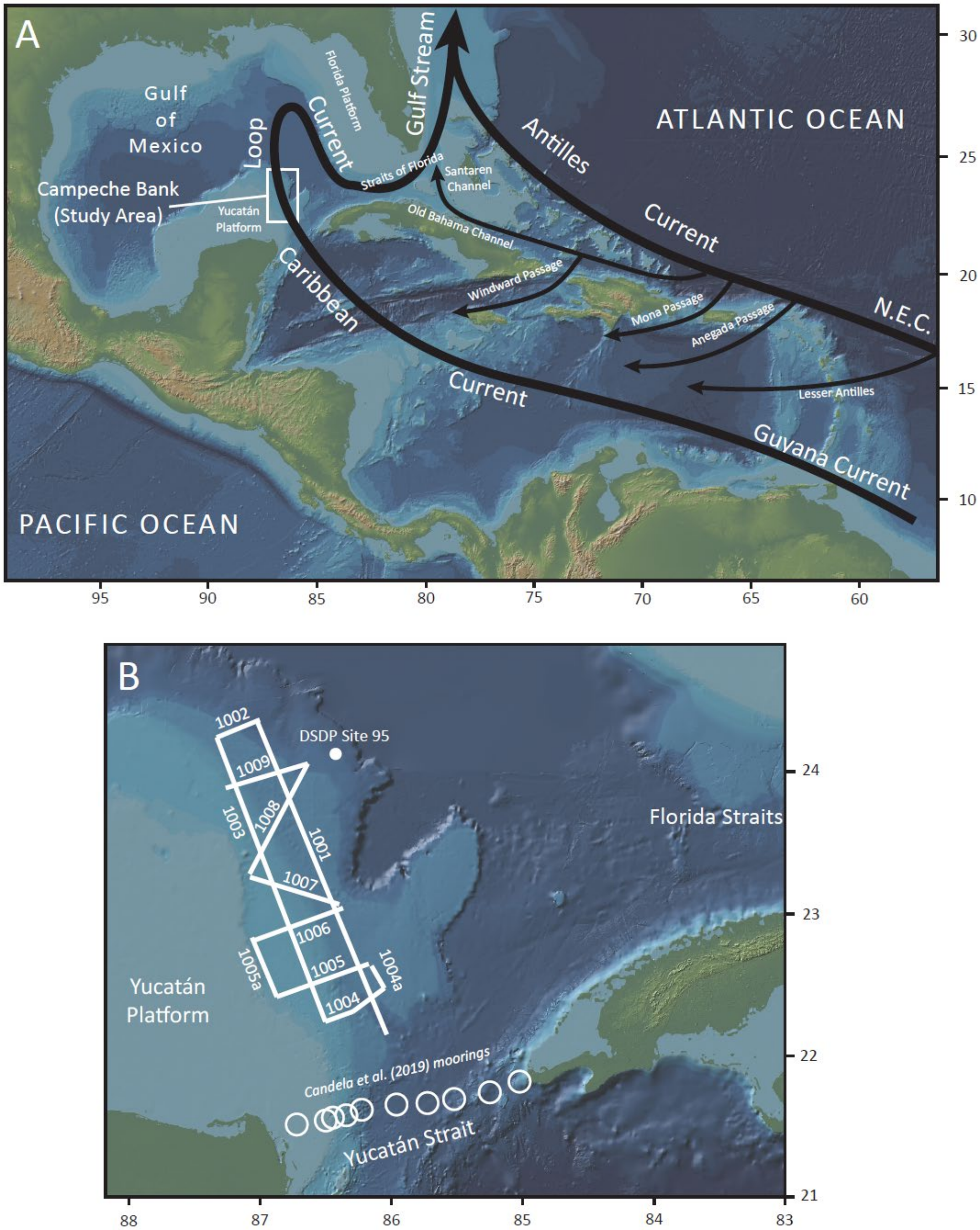

Figure 1. A) Regional surface currents associated with the North Atlantic western boundary current, including key oceanic gateways and passages for leakage of Northern Equatorial Current (N.E.C.) and Antilles Current waters into the Caribbean. B) Location map of the eastern Campeche Bank and surrounding waters, showing the location of our seismic survey, DSDP Site 95, and the mooring stations used to construct the vertical velocity profile reported in Candela et al. (2019) (Figure 2). Basemap is the Global Multi-Resolution Topography dataset (Ryan et al., 2009) plotted in GeoMapApp (www.geomapapp.org) / CC BY.

Miocene (e.g., Steinthorsdottir et al., 2021) with no sign yet of slowing down, we must understand how the Loop Current operated during past analog climate states.

In particular, it is still unknown when the Loop Current first developed its modern characteristics. How long has a current roughly the size and strength of the Loop Current been established in the Gulf of Mexico? The general consensus is that the inception and subsequent development of the Loop Current are closely tied to tectonic events in the Caribbean. Flow from the Gulf of Mexico into the North Atlantic dates back to the Late Cretaceous (Chen, 1965; Pinet and Popenoe, 1985), first through the Suwannee Straits cutting across northern Florida (also known as the Gulf Trough; e.g., Popenoe et al., 1987), and then, by the Paleocene, through the Florida Straits as well (Denny et al., 1994). The closure of the Suwannee Straits in the Oligocene is sometimes cited as the cause of the inception of a (proto-) Loop Current that was weaker than the modern Loop Current but, for the first time, was forced to make its namesake loop in the eastern Gulf to exit through the Florida Straits (Gardulski et al., 1991; Hine, 2013).

This proto-Loop Current is generally agreed to have strengthened significantly in the Middle Miocene around 14 Ma based on seismic stratigraphic architecture and cores from the western Florida Platform, where the southward flowing arm interacts with the seafloor (Mullins et al., 1987; Gardulski et al., 1991). This is coincident with the roughly simultaneous inception of sediment drifts in the Florida Straits (Mullins and Neumann, 1979; Mullins et al., 1980; Denny et al., 1994) and the Santaren Channel in the Bahamas (Anselmetti et al., 2000; Paulat et al., 2019). The Santaren Channel sediment drifts are well dated by ODP cores to ~ 12.3 Ma (Paulat et al., 2019). This Middle Miocene intensification is often cited as the start of the “modern” Loop Current (e.g., Gardulski et al., 1991; Denny et al., 1994).

However, the driver for this Middle Miocene current intensification is unclear. Many older studies associated it with the closure of the Central American Seaway (e.g., Mullins et al., 1987; Gardulski et al., 1987; Denny et al., 1994; Roth et al., 2000), but improved dating and comparison of deep-sea cores on either side of the Panamanian Isthmus have shown that closure of the Central American Seaway postdates the Middle Miocene (see review by O’Dea et al., 2016). The closure of the Central American Seaway proceeded in stages, with a closure of deep-water flow beginning in the Late Miocene between 9.8 and 7.0 Ma and a final closure to surface flow with the formation of the Isthmus of Panama in the mid Pliocene, around 2.8 Ma (O'Dea et al., 2016). Surface flow is the important aspect of this closure for the Loop Current, as the flow of warm, salty Caribbean surface water to the Pacific was blocked and redirected north where it flowed around Cuba into the Gulf of Mexico through the Yucatán Strait to the west and through the Santaren Channel to the east. If the closure of the Central American Seaway was the principal trigger for the formation of the Loop Current, this implies that the Loop Current formed around the mid Pliocene.

Evidence for increased current flow in the mid Pliocene exists on both sides of Cuba. Increased seafloor scouring (indicated by an increase in coarse fraction percentage in sediment cores) has been observed in the Yucatán and Florida Straits in the mid Pliocene (Brunner, 1984). On the western margin of Great Bahama Bank near the junction with the Florida Straits, a significant mid Pliocene shift in current flow characterized by a major increase in erosion is observed in drift deposits in Santaren Channel (Anselmetti et al., 2000). But these changes occur within drifts which all date back to the Middle Miocene, and it seems that the closure of the Central American Seaway likely only briefly invigorated an already strong current (Paulat et al., 2019).

Other Caribbean gateway changes occur or are thought to occur in the Middle Miocene, including the opening of ocean gateways in the Antilles, although these were always open to surface flow (e.g., Pindell and Kennan, 2009), and the foundering of the Northern Nicaraguan Rise carbonate "megabank" (e.g., Droxler, 1998; Roth et al., 2000; Mutti et al., 2005). The latter event is proposed by Roth et al. (2000) to be the precipitating event in the inception of the Loop Current, which according to this model was completely blocked by the presence of this large shallow carbonate bank south of the Yucatán Strait. Calcareous nannofossil data from ODP Sites 998 and 999 show that nannofloras in the northern and southern Caribbean become more similar starting 10.7 Ma, corroborating this idea (Kameo and Sato, 2000). However, evidence for deep water flow out of the Gulf of Mexico extends back to the Eocene (e.g., Denny et al., 1994) suggests this bank was not an impairment to flow from the Caribbean to the Gulf, and in any case this hypothesis cannot account for the Middle Miocene development of sediment drifts in the Bahamas (e.g., Anselmentti et al., 2000), which would have been unaffected by the Nicaragua Rise "megabank." All in all, a tectonic trigger for the inception of the Loop Current is not supported by current data.

The Middle Miocene is also associated with progressive cooling of the Miocene Climate Transition (e.g., Holbourn et al., 2022), coeval with the inception of the modern Antarctic Circumpolar Current (Livermore et al., 2007) and strengthening North Atlantic Deep Water formation driving abyssal contourite development in the western North Atlantic (Knutz et al., 2008; Boyle et al., 2017). These examples of current strengthening all point to an overall invigoration of Atlantic Meridional Overturning Circulation (AMOC) of which the Loop Current is a key part. This would indicate that the initiation of the Loop Current was triggered by climate change in some earlier warm state. If this is the case, it means that a modern climate change back toward that earlier warm state could cause the Loop Current to weaken and, perhaps, cross a tipping point resulting in a fundamental change ocean circulation.

In order to identify such a tipping point, we must better constrain when the Loop Current first developed. The Campeche Bank, just north of the Yucatán Channel where the Loop Current first enters the Gulf of Mexico, is perhaps the best place to investigate the history of the Loop Current, because it records the full history of flow into the Gulf of Mexico. Other sedimentary archives of Loop Current flow on the western Florida Shelf are biased by variations in the maximum northern extent of the loop, and proxy records from that location and the Florida Straits are biased by Mississippi River outflow, whose cool fresh water dilutes the signal of warm salty Caribbean water. The eastern Campeche Bank is the only place where a pristine record of the Loop Current, as it first enters the Gulf, can be investigated.

The presence of an active sediment drift on the Campeche Bank has been known for years thanks to the pioneering work of Hübscher and colleagues on successive cruises of the *R/V Meteor* (Hübscher et al., 2010; Hübscher and Nürnberg, 2023; Hübscher et al., 2023). To reconstruct the history of this drift we carried out a multichannel seismic survey on the *R/V Justo Sierra* in July 2022 (Figure 1B). Resultant high resolution seismic profiles allow us to understand the stratigraphy of these deposits and constrain the timing of their formation. Although the paucity of sediment cores in this area makes age control tenuous, our data strongly suggest that the Loop

Current predates the closure of the Central American Seaway and may date back to the Eocene-Oligocene Transition.

2. The Loop Current

The Loop Current dominates surface circulation in the Gulf of Mexico, which it enters through the Yucatán Strait and exits through the Florida Straits (Figure 1). Rather than tracing a direct path between these two gateways, the Loop Current first flows northward into the Gulf before swinging back south, forming the loop from which it gets its name. The northward extent of this loop varies as the result of wind patterns and the position of the intertropical convergence zone (ITCZ; Poore et al., 2004; Arrellano-Torres and Amezcua Montiel, 2022). Aperiodically (every 6-11 months), this loop pinches off and forms a warm-core anticyclonic eddy that drifts west across the Gulf (e.g., Sturges and Leben, 2000; Candela et al., 2002). These eddies are associated with a number of hazards, including a drop in surface water productivity (Biggs, 1992), altered larval fish dispersion (Lindo-Atichati et al., 2012), reduced stability of shallow gas hydrates (Milkov and Sassen, 2000), and rapid intensification of tropical cyclones (e.g, Bosart et al., 1999; Jaimes et al., 2016), notably including hurricanes Katrina (Jaimes and Shay, 2009) and Harvey (Potter et al., 2019). Eddies also drive vertical mixing of deep and surface water masses in the Gulf (Welsh and Inoue, 2000). Both eddy formation and Yucatán inflow (i.e., transport of Caribbean water through the Yucatán Channel into the Loop Current) vary seasonally, with Yucatán inflow stronger in the summer (e.g., Candela et al., 2002; Rousset and Beal, 2011) and eddy formation more common in the winter (Chang and Oey, 2012). Loop Current flow and the position of the loop are also strongly influenced by eddy formation in the northwestern Caribbean (Androulidakis et al., 2021).

The Loop Current is driven by a combination of wind stress and meridional overturning circulation (Schmitz and McCartney, 1993). The water transported through the Gulf of Mexico by the Loop Current is characterized by Caribbean water masses, summarized by Rivas (2005) and in Figure 2. Below the surface the Loop Current is characterized by warm, salty Subtropical Underwater (SUW) which forms in the northern and southern subtropics where high evaporation predominates (Rivas et al., 2005). SUW is overlain by a slightly fresher surface water mass diluted

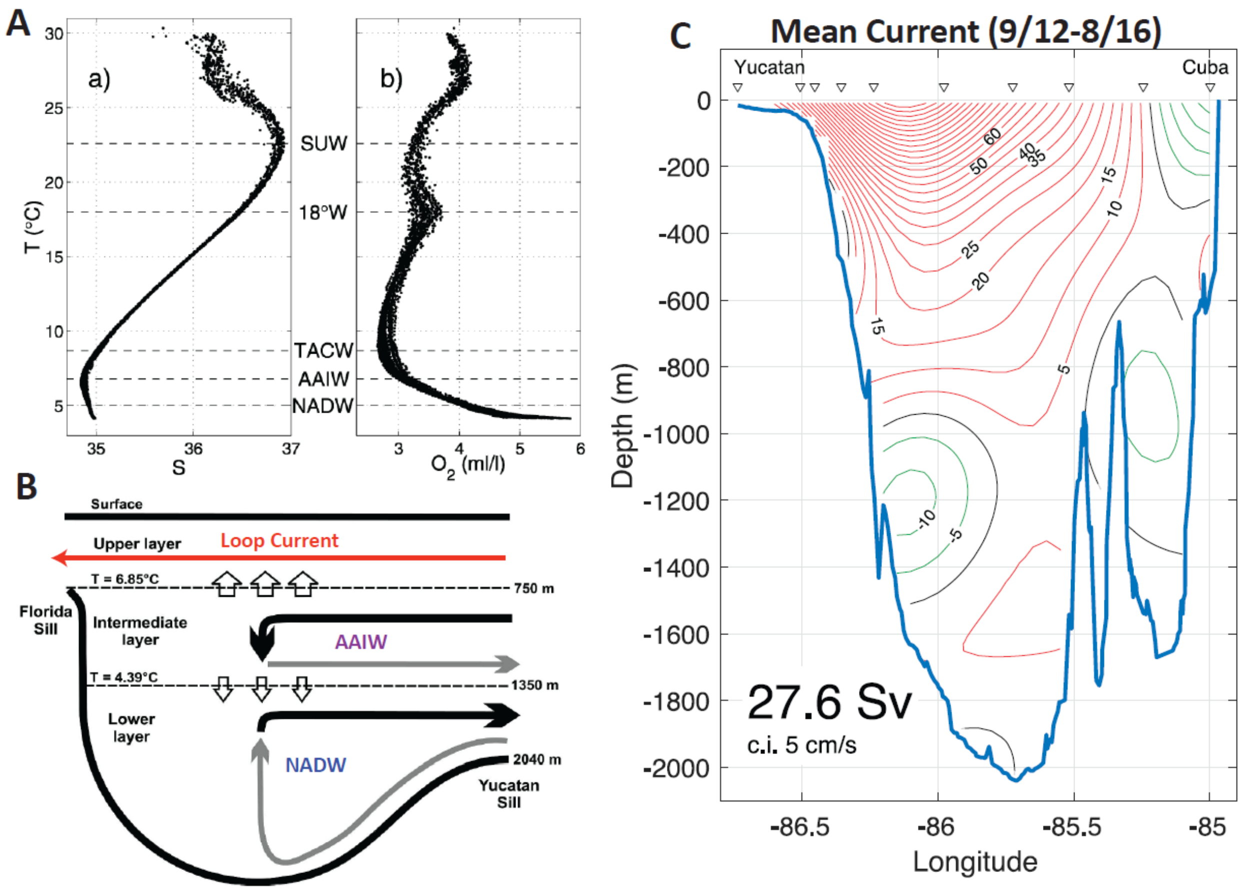

Figure 2. Southeastern Gulf of Mexico hydrography. A) Temperature (T)/Salinity (S) and Temperature/Oxygen (O_2) for Yucatán Channel from Rivas et al. (2005) showing the watermasses that enter the Gulf through this aperture; SUW: Subtropical Underwater; 18°W: 18°C Sargasso Sea Water; TACW: Tropical Atlantic Central Water; AAIW: Antarctic Intermediate Water; NADW: North Atlantic Deep Water. B) Generalized schematic of circulation through the Gulf of Mexico, modified from Rivas et al. (2005). C) Mean current velocity in cm/s through the Yucatán Channel from September 2012 to August 2016 slightly modified from Candela et al. (2019). Red contours represent northward flow and green contours southward counterflow; see Figure 1 for mooring locations.

by Amazon outflow and Caribbean precipitation (Rivas et al., 2005). Below SUW, 18°C Sargasso Seawater, characterized by an oxygen maximum, and Tropical Atlantic Central Water (TACW), characterized by an oxygen minimum, round out the upper water column down to ~ 700 m water depth (Rivas et al., 2005). The Florida and Yucatán Straits have different sill depths, with the Florida sill (~750 m) shallower than the Yucatán (~2040 m). Northward transport through the Gulf of Mexico via the Yucatán Channel and the Florida Straits is thus limited to the upper 750 m

(Rivas et al., 2005). The Yucatán Channel is the only pathway for deep water masses to enter the Gulf, which is filled by North Atlantic Deep Water (NADW) below a depth of roughly 1000 m and Antarctic Intermediate Water between 1000 m and 700 m depth (Rivas et al., 2005).

As the Loop Current enters the Gulf of Mexico through the Yucatán Channel, its "core" is 50-100 km wide, and it has a mean velocity of 1.5 m/s (with a maximum of 2.5 m/s) (Abscal et al., 2003; Ochoa et al., 2003; Badan et al., 2005; Candela et al., 2003, 2019). Moorings deployed across the Yucatán Channel by Candela et al. (2019) show that current velocity decreases as a function of depth, and the Loop Current interacts with the seafloor down to a depth of ~800 m (Figure 2) (Candela et al., 2019). A southward flowing counter current impinges the seafloor on the western side of the Yucatán Channel between roughly 1000 and 1400 m water depth (Candela et al., 2019). Mean flow into the Gulf of Mexico is 27.6 Sverdrups (Candela et al., 2019).

3. Methods

3.1 Data collection

Seismic data were collected aboard the R/V *Justo Sierra* July 15-26, 2022. This cruise was originally planned for the summer of 2020, but was twice delayed due to the pandemic. We used the Scripps Institution of Oceanography portable multichannel seismic system, which consists of two 75/75 cubic inch generator-injector (GI) air guns, a 750 m active-length Geo Eel streamer with 120 channels of 4 hydrophones each spaced at 6.25 m, and four birds for depth control. The air guns were rigged to fire in a 45 cubic inch configuration to allow an increased shot rate for higher resolution, and were towed at a depth of 3 m. In order to maintain a roughly constant speed over ground through and across the Loop Current we had to adjust our speed through the water depending on the direction we were moving; shot rate was similarly adjusted to maintain 12.5 m shot spacing, creating a common midpoint (CMP) spacing of 3.125 m. For each shot, 4 s of data were recorded at a sample rate of 0.5 ms and later resampled to 1 ms. A 50-ms layback was created during each shot due to the distance-based recording system, which was later corrected during data processing.

Our survey produced nine primary seismic profiles, labeled Lines 1001-1009 (Figure 1B). These comprise two long strike lines and seven dip lines (two of which are not perpendicular to strike due to time constraints). Additional profiles were collected along short lines connecting the ends of the main profiles. Dip lines are roughly 20 km apart and do not extend all the way to the distal edge of the Campeche Bank (a large submarine cliff called the Campeche Escarpment) because that feature lies within the Cuban exclusive economic zone (EEZ). However, our survey encompasses the large majority of the Campeche Bank drift deposits.

3.2 Data processing

We processed the data using the Paradigm application Echos with an emphasis of preserving the high-resolution nature of the survey. The processing workflow began with data importation and geometry definition. Extremely rarely during the acquisition, navigation was lost due to system glitches. The missing shot navigations are calculated using linear interpolation between existing coordinate locations. To enhance reflection amplitudes and reduce noise contamination, we applied source wavelet deconvolution using Burg's method (Burg, 1975), multichannel predictive deconvolution, a 40-320 Hz bandpass filter, trace editing, and spherical divergence correction. Bad traces were removed during trace editing. We performed velocity analysis interactively after sorting data into common mid-point (CMP) gathers; velocity functions were picked every 100 CMPs (312.5 m) to flatten coherent reflections. Additionally, we drew mutes to remove water column energy and far-offset stretching. After stacking, we used Kirchhoff post-stack time migration to collapse diffractions and restore dipping reflections to their correct positions (Yilmaz, 2001). Finally, we implemented depth conversion guided by depth-converted velocity functions.

3.3 Grain Size Analysis

To test whether there is sedimentological evidence for a change in current velocity across the Eocene-Oligocene Transition at Deep Sea Drilling Project (DSDP) Site 95 (for reasons discussed in detail below) we requested samples from Cores 2-8 (Lower Oligocene through middle Eocene; Worzel et al., 1971). These samples were soaked overnight in DI water and then run through a Mastersizer 3000 laser grain size analyzer and output at quarter-phi steps. The 10-63 µm size fraction was then plotted stratigraphically to track changes in “sortable silt,” a common proxy for bottom water current flow (e.g., McCave et al., 2017).

3.4 Data interpretation

Processed and depth-converted seismic profiles were interpreted using the Echos interpretation program for the Paradigm software package.

Ocean currents moving across the seafloor can build extensive accumulations of sediments, known as contourite drifts, so-called because they typically develop parallel or slightly oblique to continental margins, and thus follow contour lines, in contrast with down-slope currents like turbidites (Rebesco et al., 2014). As the sedimentological expressions of ocean currents, contourite deposits are exceptional archives of ocean circulation and climate history, and are typically the target of extensive sampling campaigns to understand their geometries and physical characteristics. In particular, high-quality seismic data have allowed detailed morphological categorization of contourite drifts (see review by Rebesco et al., 2014). Contourite drifts have unique internal geometries that are mappable at a seismic scale and distinguishable from stratigraphically adjacent non-contourite deposits (Faugéres et al., 1999; Nielsen et al., 2008; Rebesco et al., 2014; Boyle et al., 2017). In particular, sediment drifts tend to be bounded by erosional discontinuities that are chronostratigraphically synchronous, can be traced across the entire drift, and are typically associated with a shift in seismic facies corresponding to a shift in current strength (e.g., Faugéres et al., 1999; Rebesco et al., 2014). Horizontal or low angle dipping reflectors truncated at the seafloor or by an internal discontinuity are also common features of all sediment drifts (Faugéres et al., 1999; Rebesco et al., 2014). We used these criteria to identify and differentiate contourite drifts in our seismic profiles.

We mapped three seismic megasequences (megasequences A, B, and C) defined by unique internal characteristics and separated from each other by distinct seismic horizons that are mappable across the entire study area. Megasequences B and C were then subdivided into sequence sets based on the occurrence of internal horizons marking seismic facies change within the megasequence (Figure 3). Seismic interpretation follows previous work in the Gulf of Mexico, including Buffler et al. (1980), Angstadt et al. (1985), Denny et al. (1994), Marton and Buffler (1999), Sanford et al. (2016), Snedden and Galloway (2019), and Sickmann and Snedden (2020).

The only age control in our study area comes from an 11.4-m piston core collected by the R/V *Meteor* and dated to the Late Pleistocene by Hübscher and Nürnberg (2023). DSDP Site 95 sits a few kilometers downdip of our study area at the toe of the Campeche Bank drifts within the Cuban EEZ (and thus was not included in our survey). The Cretaceous-Paleogene (K/Pg) boundary deposit forms a bright, easily mappable reflector across the Gulf of Mexico (e.g., Buffler et al., 1980; Denne et al., 2013; Sanford et al., 2016); this event layer is also present on the eastern Campeche Bank and provides a useful marker to constrain the ages of the overlying sediments. Between this reflector and the Pleistocene core collected by Hübscher and Nürnberg (2023), we are only able to determine relative ages of the seismic units described below. Making some reasonable assumptions based on context and nearby cores, we then discuss what we interpret to be the most likely ages of these units.

4. Results

We interpret three seismic megasequences, corresponding to acoustic basement (MSA); relatively flat-lying, high amplitude reflectors (MSB); and dipping, downlapping, low amplitude reflectors separated from MSB by an erosive disconformity (MSC). MSB and MSC are subdivided into sequence sets on the basis internal facies changes and disconformities. These seismic units, their bounding horizons, internal facies, interpreted depositional environment, and age (if known) are summarized in Figure 3. Each megasequence is described in detail below. Key profiles are illustrated in Figures 4-9. Larger, higher-resolution interpreted and uninterpreted seismic profiles are included as supplemental material.

4.1 Megasequence A

Megasequence A (MSA) is the deepest seismic unit observed and therefore represents acoustic basement. Snedden and Galloway (2019) map Albian and older platform carbonates across the Yucatán Platform and around much of the Gulf rim; we interpret our MSA as corresponding to these carbonates. MSA is bounded at the top by seismic horizon H1. Reflectors of

Seismic Facies	Seismic Facies Description	Seismic Facies Interpretation	Seismic Sequence	Age	Horizon
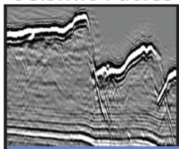	High amplitude continous reflectors drapped across a basal unconformity eroding underlying units	Active mounded contourite drifts	MSC 3	Recent-mid Pleistocene (1 Ma) (Hübscher and Nurnberg, 2023)	H6
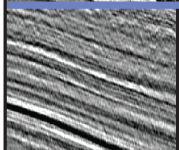	Medium to high amplitude continuous, dipping relfectors downlapping on to underlying units	Plastered sediment drift with isolated small channel features, some sediment waves, and occasional mass transport complexes. Reflectors typically downlap onto MSC1, and are truncated at the seafloor.	MSC 2	Unknown	
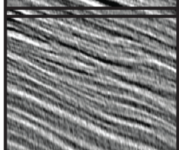	Medium to high amplitude wavy, crossbedded reflectors				
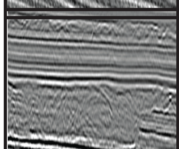	Low amplitude, chaotic reflectors sometimes eroding underlying surfaces				
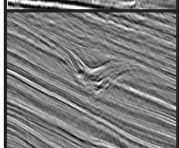	medium to high amplitude small channel features with basal erosional surface				H5
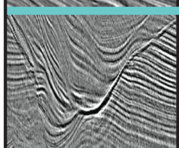	large cut and fill channels with medium to high amplitude reflectors, downlapping overbank deposits	Migrating contourite channel levee complexes. Erosive contact with underlying MSB.	MSC 1	Unknown	
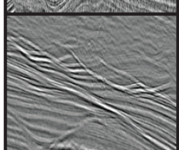	Medium to high amplitude wavy, crossbedded reflectors and amalgamated channels				
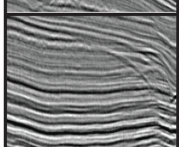	Medium to high amplitude continuous relfectors downlapping on to underlying units				H4
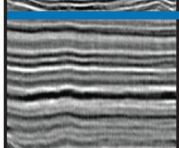	High amplitude, continous, parallel reflectors	Interbedded pelagic sediments, possibly chert-bearing	MSB 3	Paleogene?	H3
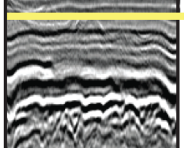	Very high amplitude incising reflectors, peak-trough-peak pattern	Mass wasting deposit associated with Chicxulub Impact	MSB 2	K/Pg boundary unit (Buffler et al., 1984; Angstadt et al., 1985; Denne et al., 2013, Sanford et al., 2016)	H2
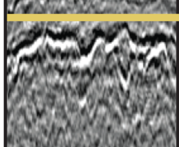	Low to medium amplitude, discontinous reflectors	Pelagic chalk	MSB 1	Late Cretaceous (Santonian-Campanian) (Worzel et al., 1971)	H1
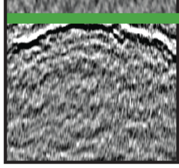	Low amplitude chaotic reflectors	Platform carbonates, acoustic basement	MSA	Early Cretaceous (Albian and older) (Worzel et al., 1971)	

Figure 3. Seismic facies, seismic units, and key horizons identified in our seismic survey. See text for description of seismic megasequences and sequence sets. Figure design inspired by Boyle et al. (2017).

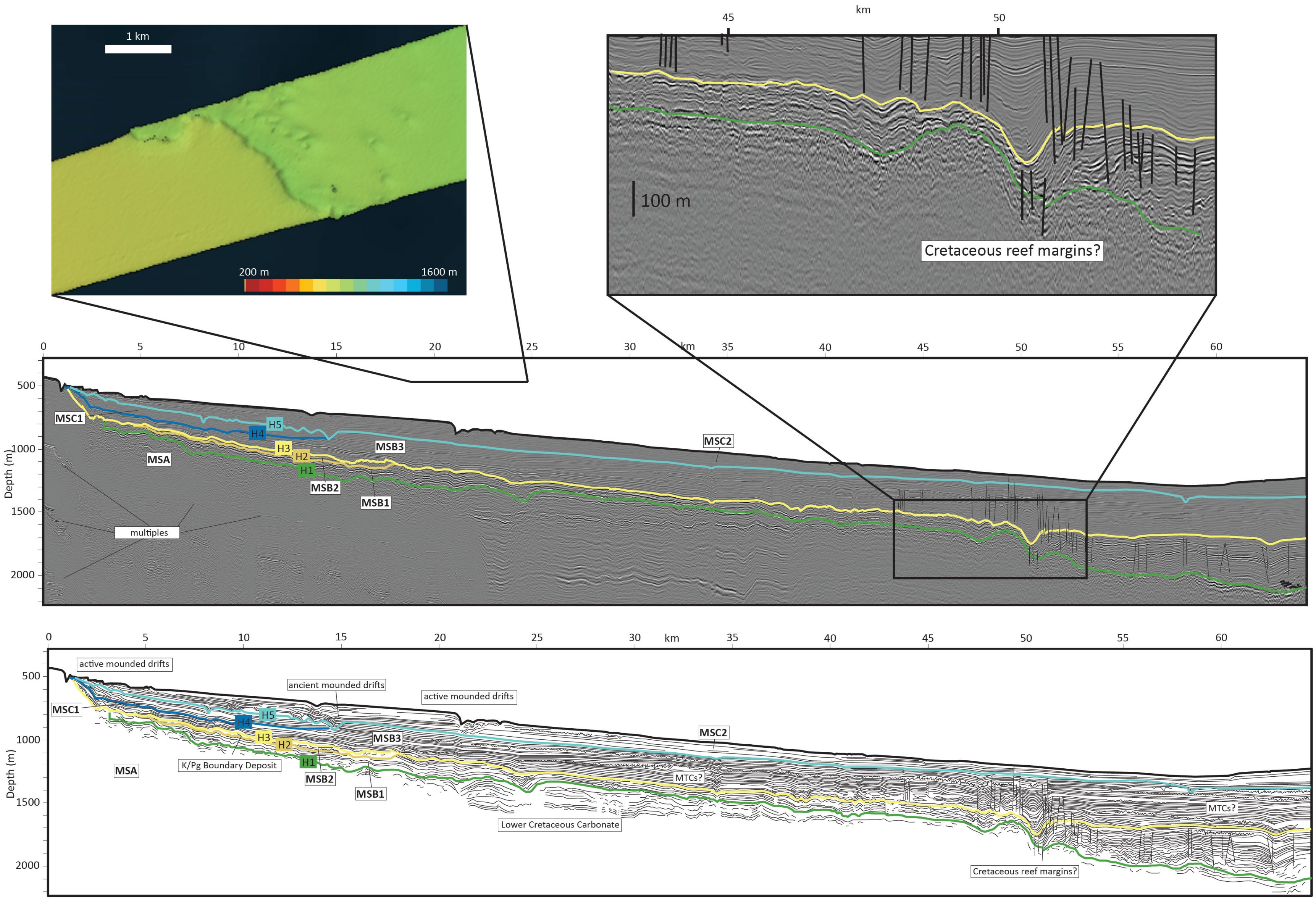

1 km
200 m
1600 m
km
45
50
100 m
Cretaceous reef margins?
Depth (m)
MSC1
H5
H4
H3
H2
H1
MSA
MSB3
MSB2
MSB1
MSC2
multiples
active mounded drifts
ancient mounded drifts
K/Pg Boundary Deposit
MTCs?
Lower Cretaceous Carbonate
Cretaceous reef margins?

306

Figure 4. Interpreted seismic profile of Line 1009, on the northern end of our study area. This profile shows relatively thinner drift deposits of MSC2, while MSC1 is limited to just the most up dip area, and MSC3 is not identified. A) multibeam bathymetry of active contourite moat in western end of profile; B) inset interpreted seismic profile showing development of reef margins in MSA (note thickening of Cretaceous pelagic sediments down dip of these margins); C) interpreted seismic profile; D) line drawing.

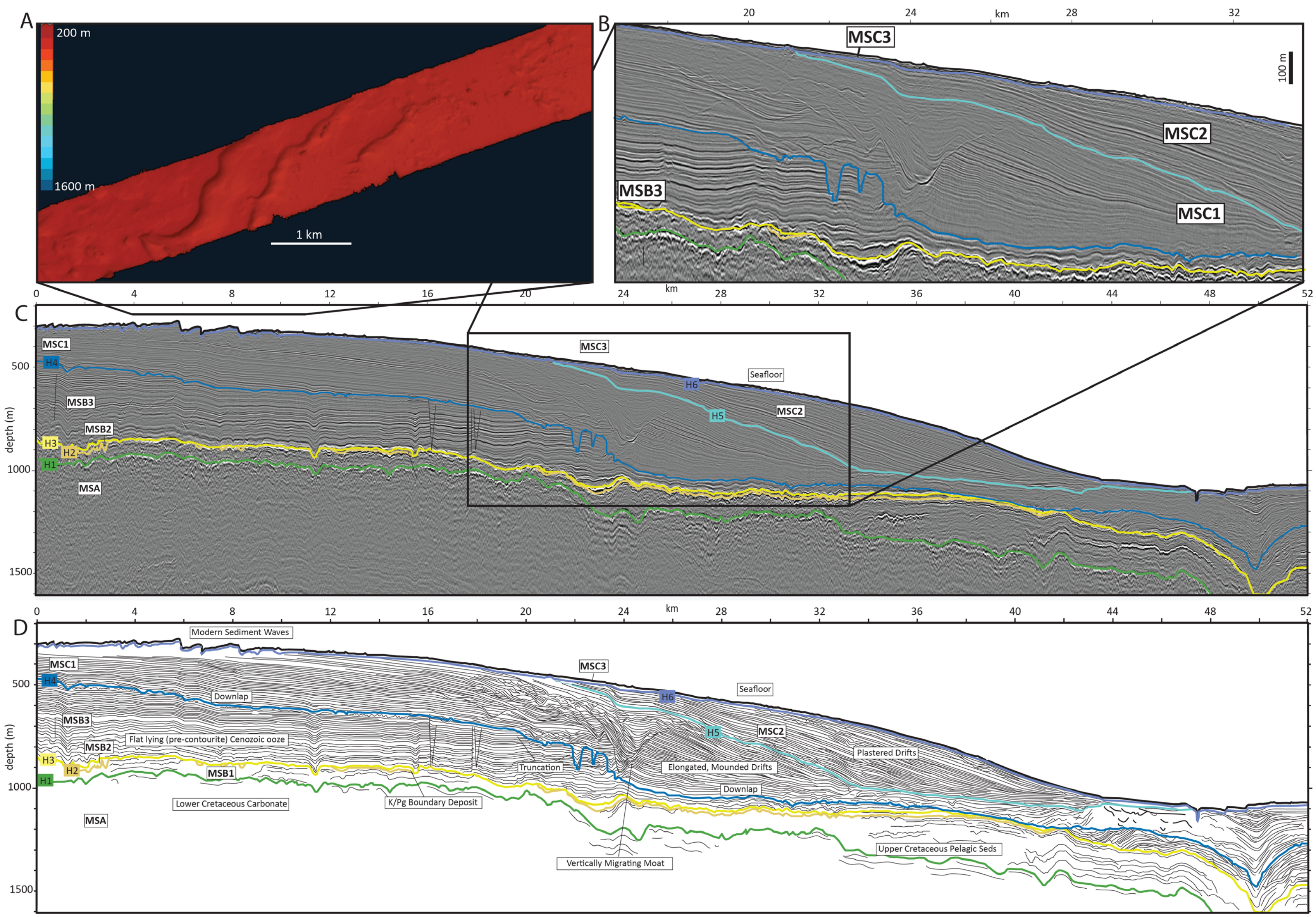
A
200 m
1600 m
1 km
B
20
24
km
28
32
100 m
MSC3
MSC2
MSC1
MSB3
C
depth (m)
500
1000
1500
MSC1
H4
MSB3
MSB2
H3
H2
H1
MSA
MSC3
Seafloor
H6
H5
MSC2
D
Modern Sediment Waves
Downlap
Flat lying (pre-contourite) Cenozoic ooze
MSB1
Lower Cretaceous Carbonate
K/Pg Boundary Deposit
Truncation
Elongated, Mounded Drifts
Downlap
Plastered Drifts
Vertically Migrating Moat
Upper Cretaceous Pelagic Seds
km
0
4
8
12
16
20
24
28
32
36
40
44
48
52

Figure 5. Interpreted seismic profile of Line 1005, which is notable for the dramatic incision of MSC1 into MSB, and for the large amalgamated channels in MSC1. (see inset). A) multibeam sonar bathymetry of sediment waves near western end of profile; B) inset interpreted seismic profile of notable erosional features in MSC1; C) interpreted seismic profile; D) line drawing of interpreted profile. See location map in Figure 1B.

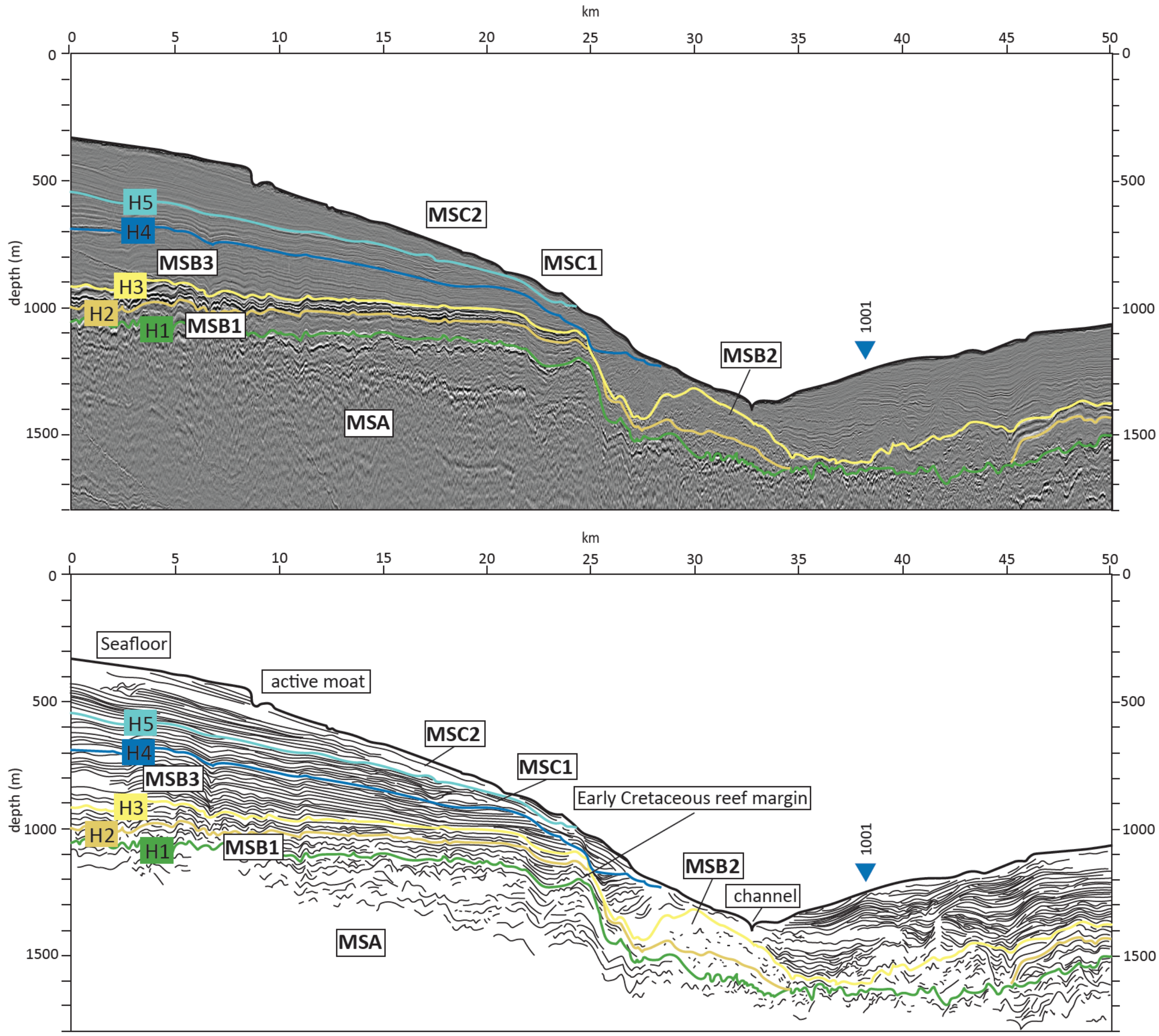

Figure 6. Interpreted seismic profile of Line 1004, on the far southern end of our study area. The Campeche Bank drift is narrower here and mostly limited to the far western area of this profile, updip of a steep early Cretaceous reef margin. Note thick K/Pg mass transport deposit at the foot of this relict escarpment. A deeper water drift complex, unrelated to the Loop Current, can be seen on the eastern end of this profile. A) interpreted seismic profile; B) line drawing of interpreted profile. See location map in Figure 1B.

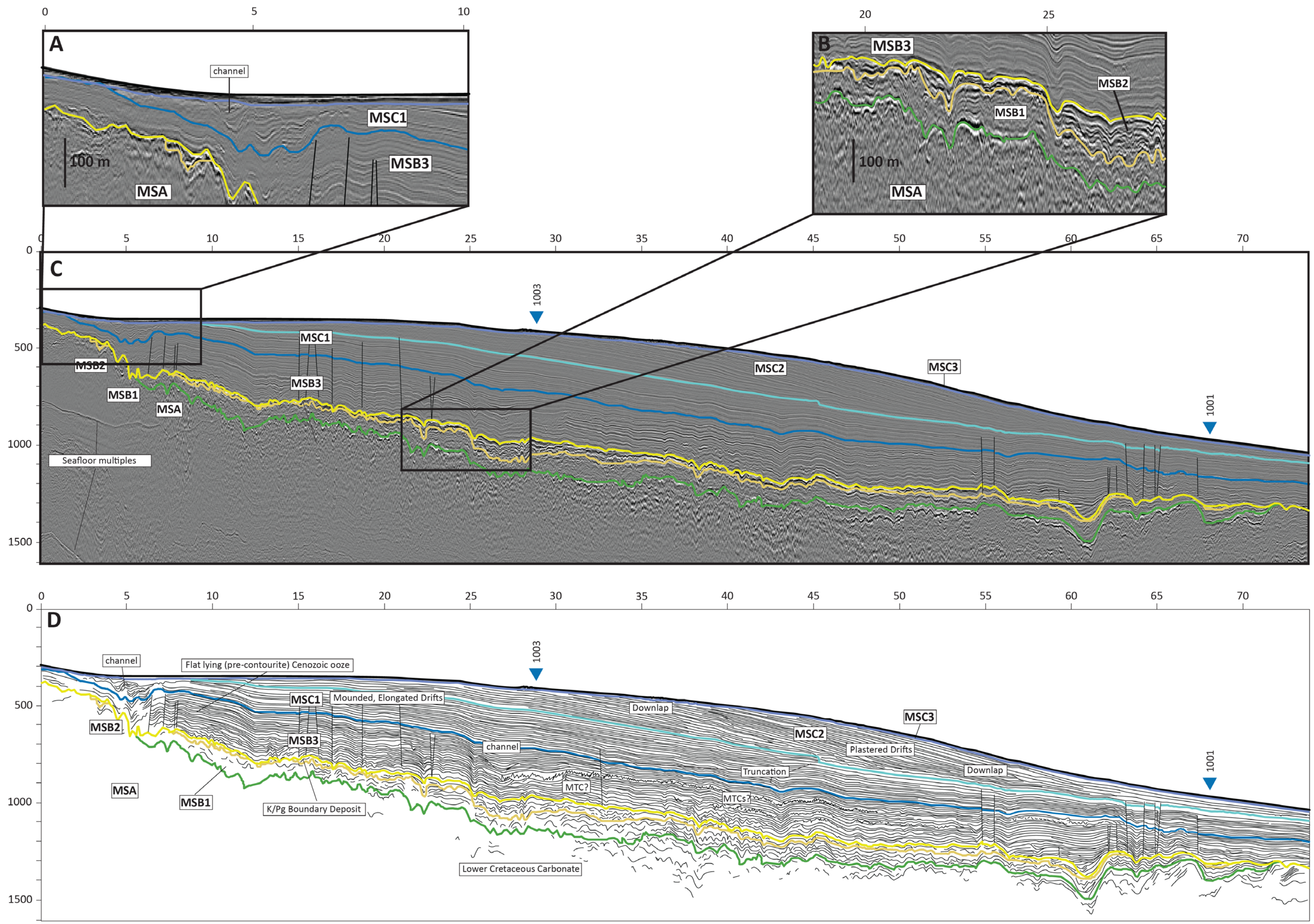
A
channel
MSC1
100 m
MSB3
MSA
B
MSB3
MSB2
MSB1
100 m
MSA
C
1003
MSC1
MSB2
MSB1
MSA
MSB3
MSC2
MSC3
1001
Seafloor multiples
D
channel
Flat lying (pre-contourite) Cenozoic ooze
MSC1
Mounded, Elongated Drifts
1003
Downlap
MSC3
MSB2
MSB3
channel
MSC2
Plastered Drifts
Truncation
Downlap
1001
MTC?
MSA
MSB1
MTCs?
K/Pg Boundary Deposit
Lower Cretaceous Carbonate

313

Figure 7. Interpreted seismic profile of Line 1006, in the central part of our study area. The Campeche Bank drift is thick but contains fewer channels than nearby Line 1005. A) An amalgamated channel complex is present at the far updip end of MSC1; B) characteristic K/Pg boundary deposit with thicker deposit with fairly thick (~100 m) build up in a paleo low; C) interpreted seismic profile; D) line drawing of interpreted seismic profile. See location map in Figure 1B.

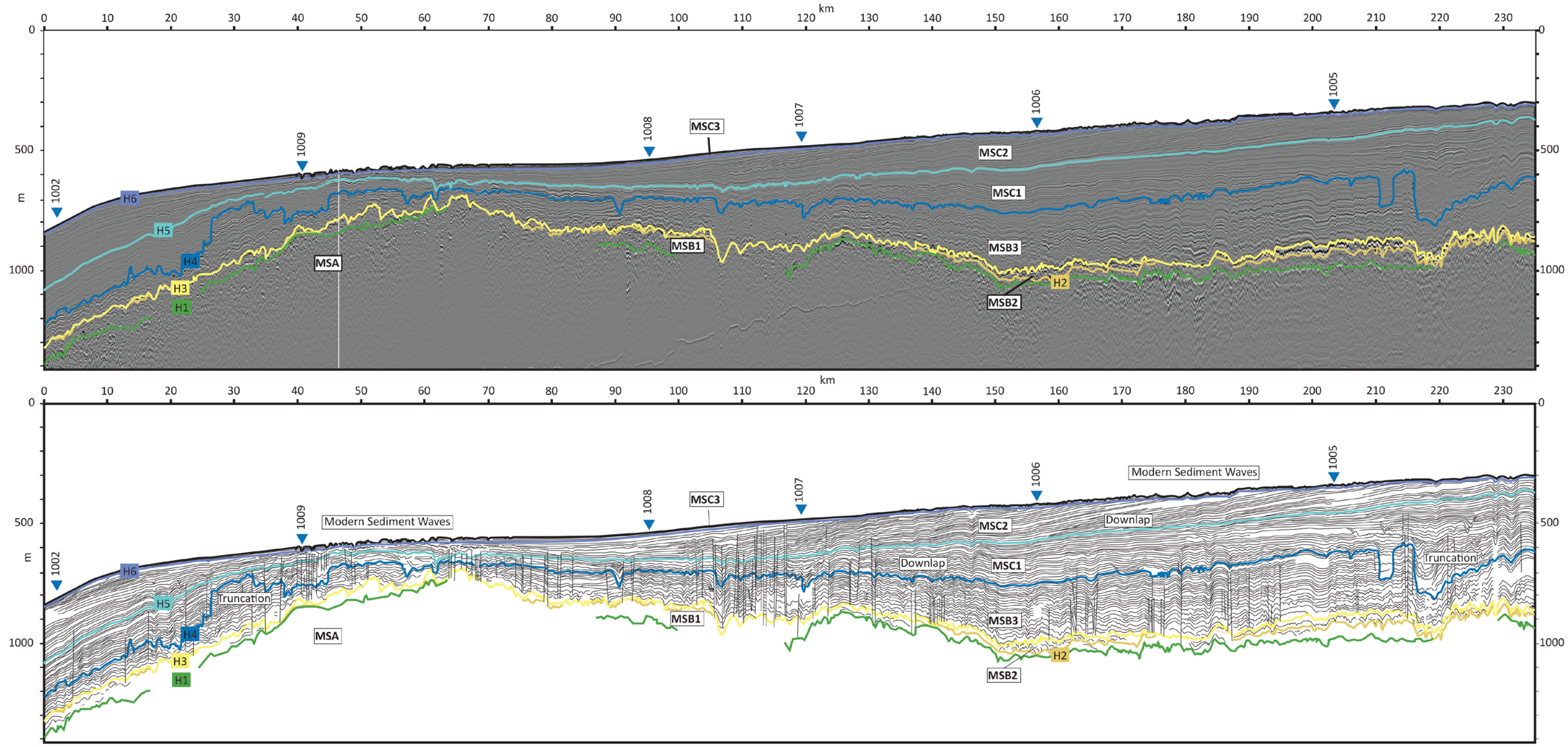

Figure 8. Interpreted seismic profile of Line 1003, the updip strike line. Northward dipping reflectors downlapping on Horizon H5 show deposition across the entire length of the contourite drift. Extensive erosion along Horizon H4 (representing the base of contourite drift deposition) is occurs across the entire profile and is particularly evident at the far northern and southern ends. A) An amalgamated channel complex is present at the far updip end of MSC1; B) characteristic K/Pg boundary deposit with thicker deposit with fairly thick (~100 m) build up in a paleo low; C) interpreted seismic profile; D) line drawing of interpreted seismic profile. See location map in Figure 1B.

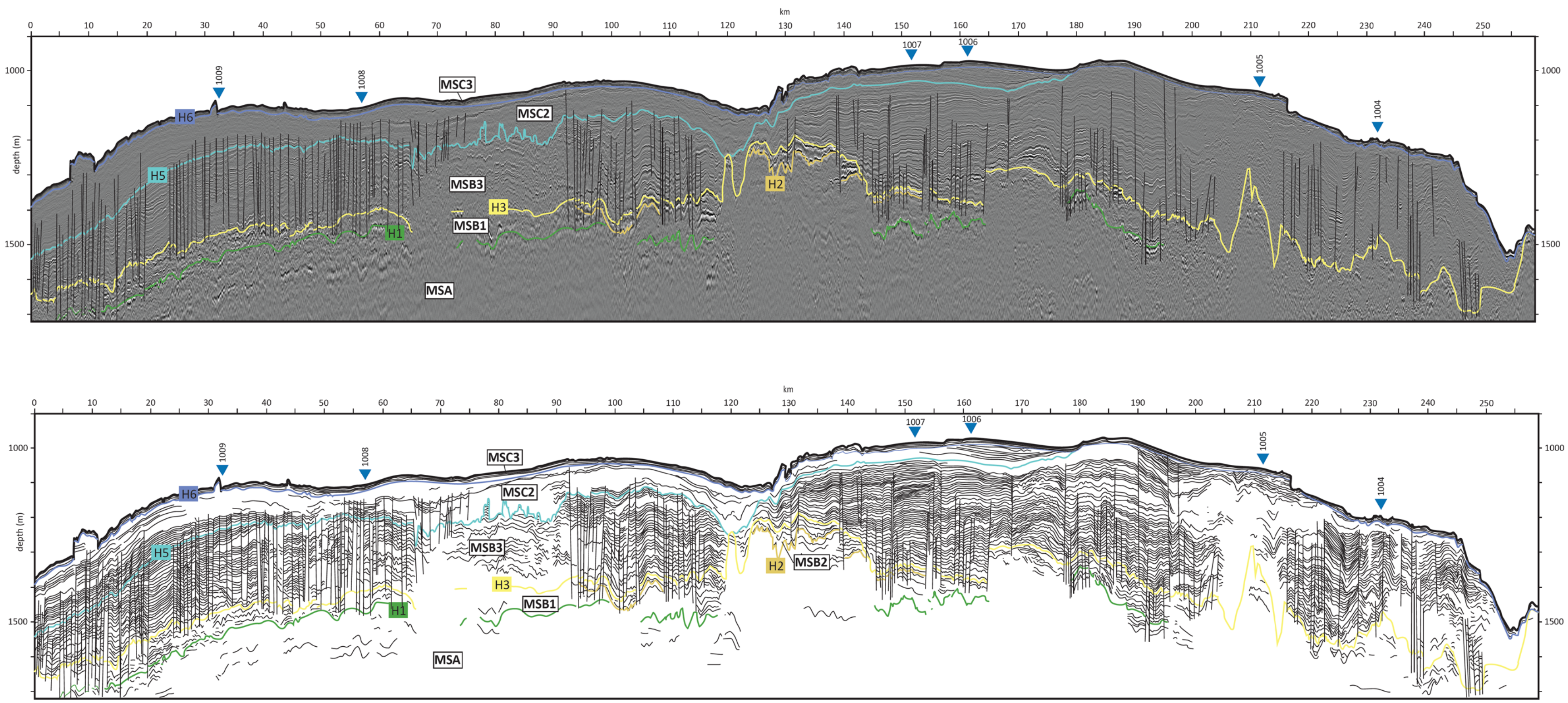

Figure 9. Interpreted seismic profile of Line 1001, the downdip strike line. Of particular interest in this line is the erosional escarpment on the southern end, facing the Campeche Channel. Even below 1000 m there appears to be active erosion at the seafloor. A) interpreted seismic profile; B) line drawing of interpreted seismic profile.

the overlying MSB1 onlap and, in places, downlap on this horizon. MSA is characterized by low amplitude, chaotic reflectors. In some places, mounded geometries are present within the unit (Figure 3); these mounded geometries are often associated with a corresponding mound in horizon H1, along with an increase in slope in the downdip direction. These features are best developed in Line 1009 (Figure 4), and we interpret them to represent reef margins.

No core penetrations of MSA exist within our study area. At nearby DSDP Site 95, drilling recovered Early Cretaceous (Albian and older) dolomitized carbonates from an ancient shallow water carbonate platform which drowned as the basin subsided and sea level rose in the mid Cretaceous (e.g., Buffler et al., 1980). This age and depositional environment agrees with the regional interpretations of Snedden and Galloway (2019). The flat-lying, high amplitude reflectors observed in the deepest part of MSA along Line 1009 (Figure 4) may represent anhydrite deposits, which are known from the Aptian of both the Yucatán and Florida platforms, as well as the Bahamas (Austin et al., 1986; Ward et al., 1995; Snedden and Galloway, 2019).

4.2 Megasequence B

Megasequence B (MSB) is comprised of parallel reflectors (sometimes subparallel, due to interpreted faulting and folding) (Figure 3). These reflectors onlap onto seismic horizon H1, which separates MSB from MSA. The upper contact with the overlying MSC is defined by seismic horizon H4; this contact is characterized by an erosional unconformity across most of the study area. In some places roughly parallel reflectors above and below H4 give it the appearance of a paraconformity. In other places (best developed in Line 1005; Figure 5) this horizon H4 is characterized by obvious erosion and incision, sometimes of more than 100 m. The parallel reflectors of MSB are interpreted to indicate Late Cretaceous to Cenozoic pelagic sedimentation without any evidence of contourite deposition. These pelagic sediments are divided by the K/Pg boundary deposit, a layer of erosion and mass wasting 10s to 100s of m thick bounded by seismic horizons H2 and H3. This bright, easily mappable event deposit splits MSB into three interpreted sequence sets: MSB1 (Cretaceous pelagic sediments), MSB2 (K/Pg boundary deposit), and MSB3 (early Cenozoic pelagic sediments).

4.2.1 Megasequence B1

Megasequence B1 sits unconformably on top of the interpreted relict carbonate platform and reef margins of MSA. Onlapping reflectors are evident at different positions along this contact (particularly along lines 1005 and 1009). This unit gets progressively thicker down dip, and older MSB1 reflectors exist down dip of relict reef margins of MSA, possibly indicating active pelagic sedimentation in deeper waters prior to platform drowning. Some small normal faults (with offset on the scale of tens of meters) occur in the thickest sections of MSB1 (see distal end of Line 1009, Figure 4). Compared with MSB3, the reflectors of MSB1 are thinner, lower amplitude, and more discontinuous (Figure 3). The parallel nature of these reflectors marks them as the result of pelagic sedimentation without the influence of any significant bottom water current. A single interpreted mass transport complex (MTC) occurs in the upper part of this MSB1 in the most distal section of Line 1009 (Figure 4), indicating sufficient deposition up dip to result in slope failure. Thick up dip deposits of MSB1 do not occur in our study area, and we conclude they must have been erased by the mass wasting that occurred following the Chicxulub impact.

At nearby DSDP Site 95, Santonian to Campanian pelagic chalks were recovered between the K/Pg boundary deposit and underlying Early Cretaceous platform carbonates (Worzel et al., 1973). Up dip of the thin deposits at Site 95, it is possible that some of the pelagic sediments overlying Early Cretaceous carbonates date as far back as the early Turonian, when the Yucatán platform drowned (Anotine et al., 1974; Shaub, 1983; Sohl et al., 1991; Snedden and Galloway, 2019).

4.2.2 Megasequence B2

Megasequence B2 is characterized by two very high amplitude reflectors, defined here as horizons H2 (bottom) and H3 (top) (Figure 3). In some places the unit is so thin that the two reflectors merge into one; this is mapped as horizon H3, which represents the top of this deposit. The base of this sequence is sometimes paraconformable but more often truncates underlying strata. Overlying strata are conformable or sometimes onlap. Both the top and bottom of MSB2 represent uneven surfaces, especially along strike, and can vary vertically by >100 m over a distance as short as a kilometer. MSB2 is also of uneven thickness; sometimes Horizons H1 and H2 are so close together they form a single reflector separating MSB1 and MSB3, and other times they are separated by chaotic, often lumpy reflectors of variable amplitude. This internal chaotic unit can be up to 200 m thick (as is the case in Line 1004, Figure 6; other especially thick accumulations occur in Line 1006, Figure 7; and Line 1001, Figure 9) and are interpreted to represent large slump deposits.

The K/Pg boundary deposit is well-known and easily mappable seismic reflector across the entire Gulf of Mexico Basin. Originally mapped as the Mid Cretaceous Unconformity (because earliest Cenozoic sediments unconformably overlie middle Cretaceous sediments; e.g., Buffler et al., 1980), the discovery of the Chicxulub Crater by Hildebrand et al. (1991) cast this unit in a new light. The Chicxulub impact released a massive amount of energy into the Gulf of Mexico. Seismic waves led to the collapse of whole sections of the margins of the Florida and Yucatán platforms, and the multiple tsunami which followed immediately after the seismic waves led to further mass wasting (e.g., Sanford et al., 2016). The K/Pg boundary deposit itself is composed of a chaotic mixture of Cretaceous and older sediments jumbled together during their (re)deposition (e.g., Bralower et al., 1998). At DSDP Site 95, the K/Pg boundary unit is only about 3 m thick (Lowery and Bralower, 2022), likely due to its position at the edge of the Campeche Platform. With little accommodation above the Campeche Escarpment much of the material likely continued moving downslope to make up the much thicker deposits in the adjacent deepwater. DSDP Sites 540 and 536, both deposited on paleo highs below the Campeche Escarpment, have K/Pg boundary deposits around 50 m thick while deposits more than 100 m thick are evident in nearby seismic data (Sanford et al., 2016).

With the exception of a few local slumps and depressions filled with material, the K/Pg boundary deposit on the Campeche Bank is generally thin and represented by just one or two reflectors. Truncation of underlying reflectors indicates that significant erosion occurred, and this material must have been transported off the Campeche Bank and into the thick K/Pg boundary deposits in the deep water to the east.

4.2.3 Megasequence B3

Megasequence B3 is primarily comprised of high amplitude parallel reflectors (Figure 3). MSB3 sits conformably on top of the K/Pg boundary deposit (MSB2), with basal reflectors onlapping that event layer. Some small, incised channels exist in MSB3. These channels tens of meters thick and a few hundred meters wide; they erode underling strata, are infilled by one or two cross-bedded reflectors, and are overlain by flat lying reflectors that extend beyond the channel. They occur rarely in MSB3, with just a handful of widely spaced channels in any one profile. The largest channel we observe in MSB3 is <100 m thick and ~1 km wide (Line 1006; Figure 7). Packages of chaotic, low-amplitude reflectors also occur throughout MSB3, and are interpreted as mass transport complexes (MTCs) (e.g., Line 1009, Figure 4; Line 1006, Figure 7). Generally, these units have a thickness on the scale of 10s of meters, often just replacing a flat, high amplitude reflector with a chaotic, low amplitude reflector, but not disrupting layers above and below. Rarely, they truncate underlying strata. These MTCs are laterally extensive, sometimes stretching 10s of kilometers.

MSB3 is truncated by Horizon H4. Across much of the study area this contact appears conformable, particularly in downdip areas. Up dip, truncation of underling strata is evident, although often at a fairly low angle. A major exception to this trend occurs in Line 1005 (Figure 5), where extensive erosion is evident in the form of several narrow (several hundred meters wide), deep (~100 m) incised channels and an erosional scarp representing ~300 m of strata truncated and exposed at the paleo seafloor represented by H4. The nature of these channels is discussed in Megasequence C1, below. This erosion is well-expressed on both the northern and southern ends of the two strike lines we collected, where the high amplitude reflectors of MSB3 are truncated (sometimes with 100s of meters of erosion) by the low amplitude reflectors of MSC1. Line 1003 (Figure 8) also clearly shows the high amplitude parallel reflectors of this unit and extensive erosion by Horizon H4.

We interpret the high amplitude, roughly flat-lying reflectors of MSB3 to represent early Cenozoic pelagic sedimentation in the near absence of any currents moving sediments along the seafloor. Weak but erosive contourite currents are evident from the small channels that occur intermittently through MSB3, but as these features are rare, it appears the seafloor was generally quiescent at this time. This quiescence was brought to an abrupt end at the transition to Megasequence C.

4.3 Megasequence C

Megasequence C (MSC) is composed of low to high amplitude, parallel, wavy, dipping, and cross-bedded reflectors (Figure 3). Its lower contact with MSB is erosional (as discussed above; Horizon H4) and characterized by downlapping reflectors onto the erosional surface. A second erosional surface (Horizon H5) occurs partway through the unit, also characterized by downlapping reflectors. This transition marks a shift from parallel reflectors with channel features (MSC1) to dipping reflectors which come together on a common downlap surface (MSC2), and which are truncated in the updip direction by a third erosional surface (Horizon H6) just below the modern seafloor. Between this upper erosional surface and the seafloor is a thin (10s of m) unit with very low amplitude reflectors (MSC3). The seafloor itself is characterized by features indicative of modern contourite flow: incised moat channels and downdip drift deposits (Figure 4, Figure 8). The widespread erosional surfaces that can be traced across the entire drift are characteristic of contourite deposits (Faugères et al., 1999). Overall, MSC records the inception and development of contourite drift deposition on the Campeche Bank, from elongated contourite drifts (MSC1) to plastered drifts (MSC2) to modern moat and drift deposits (MSC3). MSC3 is mid Pleistocene to Recent according to Hübscher and Nürnberg (2023), but no age control exists for MSC2 or MSC1.

4.3.1 Megasequence C1

Throughout most of the study area, Megasequence C1 is characterized by medium to low amplitude continuous reflectors downlapping on underlying units (Figure 3). In some areas, particularly to the south (and best expressed in Line 1005, Figure 5), it also contains discontinuous, medium to low amplitude, wavy, crossbedded reflectors, small scale amalgamated channels, and very large amalgamated channels with downlapping overbank deposits. MSC1 thins to the north, and is only present in the updip section of the northern profiles, and then only with a maximum thickness of ~100 m. A basal erosive disconformity separates MSC1 from MSB3 (Horizon H4).

Although they are the least dramatic, the low to medium amplitude, continuous, downlapping reflectors are the most common facies in MSC1. They are thickest in the updip sections of Lines 1004, 1005, and 1006 (Figures 5-7). In Line 1005 they transition laterally into the large, amalgamated channel deposits that make up the most striking part of MSC1 in that profile; individual reflectors can be traced into channel deposits before terminating against the channel wall or being truncated by another channel (Figure 5).

The largest of these channels are up to 400 m thick and several kilometers wide. These prominent erosional features cut deep into MSB3, and the overall erosion of underlying strata is on the order of hundreds of m. These channels erode updip strata and redeposit it downdip in overbank deposits that pinch out toward a common downlap surface, tracking the progradation of the drift deposits. Amalgamated channels along a structural high with levee deposits downdip is the classic geometry of elongated contourite drifts (e.g., Rebesco et al., 2014). In Line 1005, these channels start out very narrow and deep, get slightly wider and much deeper, and then get progressively wider and shallower upsection (Figure 5). As this transition occurs, lateral distribution of the channels widens, too. Instead of being concentrated in a narrow deep channel, the bottom water current was spread out over a wider area of the ancient seafloor. This results in the third seismic facies that characterizes MSC1: low to medium amplitude wavy, cross-bedded reflectors and amalgamated channels.

Almost as striking as the geometry of these large erosional complexes is the fact that they only occur at this impressive scale in a single line (1005, Figure 5). The wide line spacing in our survey design allows us to characterize the overall stratigraphy of the whole drift but precludes mapping interesting localized features like these channels. The only other airgun seismic survey in this area (Hübscher et al. 2023) did not find any large channel features, although it had even fewer lines than our own survey. This combined result of limited areal extent of large channel deposits in MSC1 suggests that the strong current flow transitioned from a channel-confined contourite on the southern end of the margin to a surficial drape resulting from the strong deceleration of the bottom currents once they passed over this southern rampart. It is possible that the facies change from MSC1 to MSC2 is the result of changing slope morphology, gradually smoothing out and allowing more unimpeded flow across the whole Campeche Bank. To the north, a moat channel occurs in MSC1 at the foot of the Yucatán carbonate platform in Line 1006 (Figure 7), but this is much smaller than the massive channels in Line 1005 (Figure 5).

4.3.2 Megasequence C2

Megasequence C2 (MSC2) is characterized by medium to low amplitude dipping reflectors and is separated from MSC1 by a basal erosive disconformity (Horizon H5) (Figure 3). These dipping reflectors can be parallel and continuous, wavy and cross bedded, or cut by small channels. They thin in the downdip direction and downlap onto the basal erosive disconformity separating MSC1 from MSC2. These reflectors also thin in the updip direction, where they are truncated by the basal erosive disconformity of MSC3 (Horizon H6). Thick in the middle and thin on the ends, MSC2 forms an overall elongated lens of sediment characteristic of a plastered sediment drift (e.g., Rebesco et al., 2014). Within this lenticular deposit, a variety of facies associated with contourite flow are apparent. There are small channels (10s of m deep and 100s of m wide, much smaller than their larger predecessors in MSC1), wavy or hummocky cross bedding, and local onlap surfaces present. These features are more common in the thicker and more steeply dipping sections in Lines 1005 and 1006 (Figures 5 & 7), whereas only a few channels and wavy bedding surfaces are present to the north in Line 1009 (Figure 4). Although large (100 m tall) active moats associated with modern contourite flow are present on the seafloor (mapped as MSC3), no channels or relict moats of similar scale are visible in MSC2. In the northern part of the study area, MSC2 directly overlies the pre-drift deposits of MSB3 except in the most updip areas. It is unclear whether MSC1 was originally present and then erased by subsequent erosion associated with the basal disconformity of MSC2.

4.3.3 Megasequence C3

Megasequence C3 is a thin unit associated with the modern seafloor and a thin drape of sediments separated from MSC2 by a basal erosive disconformity (Horizon H6) (Figure 3). At the vertical resolution of our seismic data, it is a few reflectors thick, corresponding to 20-30 m of sediment. Although the internal structure of MSC3 is difficult to resolve in our data, we can clearly see the truncation of underlying strata by the basal disconformity.

Hübscher and Nürnberg (2023) surveyed this unit with high resolution single channel parasounder data in the central and northern parts of our study area and were able to image the internal structure clearly. They found sub parallel reflectors which onlap onto the underling basal disconformity; sediments are thickest in the middle and thin updip and downdip (Hübscher and Nürnberg, 2023), forming a wedge of sediments that looks like MSC2 in miniature. They also found sediment waves similar to those on the modern seafloor. Hübscher and Nürnberg (2023) also report the results of several sediment cores taken from within this unit, the oldest of which extends back to Marine Isotope Stage 11 (~400 ka). Extrapolating this sedimentation rate to the basal erosive disconformity, they find an age of ~1 Ma, coincident with the Mid Pleistocene Transition (MPT) (Hübscher and Nürnberg, 2023).

The modern seafloor is characterized by a number of features indicative of ongoing contourite flow, particularly moats, which are evident in both multibeam and MCS data (Figures 4-6). These moats can be on the scale of 100 m, much larger than any channels observed in the underlying MSC2. Moats tend to occur between 300 and 600 m water depth.

On the southern end of the Campeche Bank, the deeper seafloor (below ~1100 m) is characterized by erosion, as a 300 m tall scarp faces directly into the oncoming current (Line 1001, Figure 9), while deposition occurs across the northern end of the line. We also note the presence of a narrow, ~50 m deep channel around 1300 m water depth in the saddle connecting the Yucatán Strait to the top of Catoche Tongue (Figure 5-6). These down dip erosional features are much too deep to be influenced by the Loop Current, which extends down only to ~ 800 m (Candela et al., 2019), and we interpret them to be the result of NADW flow into and out of the Gulf of Mexico. This is the depth of the southward-flowing counter current evident in the mooring observations of Candela et al. (2019) (Figure 2).

5. Interpretations

The onset of contourite deposition occurred at the base of MSC1, marked by a major erosional event and representing the transition from parallel, continuous, high amplitude reflectors to a package of medium to low amplitude reflectors characterized by a range of indicators of bottom water currents (amalgamated channels, wavy, cross bedded reflectors, dipping and downlapping reflectors, etc). We interpret this inception of contourite drift deposition to mark the onset of the Loop Current in something like its modern form. The lack of age control within these units means that we can only say for sure that the Loop Current developed sometime between the K/Pg boundary and the Mid Pleistocene Transition (so, some 65 myr). By making a few assumptions about the geologic context we can narrow that down significantly.

5.1 Loop Current Development

The stratigraphy of the Campeche Bank is characterized by Early Cretaceous carbonates and then Late Cretaceous and Cenozoic pelagic sediments prior to the development of large contourite deposits sometime in the Cenozoic. The lack of large scale contourite deposits below MSC1 indicates that a current with the speed and depth of the modern Loop Current did not exist prior to Horizon H4, but the occasional presence of smaller scale strike-parallel channel features in MSB3 suggests some contourite current flow across the Campeche Bank in the early Cenozoic, and thus exchange of water through the Yucatán Strait at this time.

Phase 1: Initiation of Contourite Deposition; Mounded Elongated Drifts

The shift from pre-contourite to contourite deposits on the Campeche Bank is stratigraphically sharp, with the flat-lying strata of MSB3 incised hundreds of meters by channels and other erosional features at the base of MSC1. This erosion is most apparent at the southern end of the Campeche Bank (Figure 5, Figure 9) but the basal disconformity (Horizon H4) is mappable across the entire survey area. This implies a rapid development of a strong, deep current that eroded existing sediments. This event may have been less instantaneous than it appears seismically, since the evidence of a ramp-up in current flow could have been erased by subsequent erosion, and without age control from cores it is impossible to know how much missing time is represented in the disconformity. It is also possible that a proto-Loop Current existed that did not impact the seafloor across the Campeche Bank, and that the onset of contourite deposition tracks the *deepening* of that current, rather than its initiation. These are both questions that require sediment cores to answer properly. Regardless of how fast, exactly, the transition to contourite deposition took, the base of MSC marks a major shift in the hydrography of the waters overlying the Campeche Bank and in the stratigraphy of the sediments deposited across it below 800 m water depth. This signals the development of a current similar in velocity and depth profile to the modern Loop Current.

The large erosional features which characterize MSC1 in Line 1005 slowly transitioned from narrow deep channels to wide, shallow channels (Figure 5). This marks either a reduction in current velocity or, more likely, a gradual reshaping of the slope as erosion slowly redeposited sediments to better accommodate contourite current flow.

Phase 2: Transition to Plastered Drifts

A more important change occurs with the transition from MSC1 to MSC2, marked by a second widespread erosional disconformity (Horizon H5). Erosional disconformities mark a change or break in contourite current flow, typically associated with an increase in current velocity driving widespread erosion across the contourite drift (Faugères et al., 1999; Rebesco et al., 2014). The erosion along this disconformity is not as dramatic as that at the base of MSC1 and is primarily expressed as either truncation of underlying strata or small channel features. This marks a change from elongated contourite drifts characterized by channel features and overbank deposits (i.e., “elongated mounded drifts;” Rebesco et al., 2014) in MSC1 to plastered contourite drifts developing along the slope without large moats up dip in MSC2. Some small moats do occur in MSC2 in the northern end of the study area, but they are fairly small compared to the moats in MSC3 or the modern channels in MSC1.

According to the contourite drift taxonomy of Faugères et al. (1999), plastered drifts can occur on a slope at any depth, “where gentle relief and smooth topography favor a broad non-focused bottom current” (p. 10). This seems to be the case with MSC2, where the main change is a gentler slope compared to MSC1, which could facilitate the shift from mounded drift to plastered drift without any reduction in current velocity. Indeed, there must have been an increase in velocity to create the basal disconformity of MSC2 at Horizon H5, although this increase could have been ephemeral.

Phase 3: Transition back to Mounded Elongated Drifts

Another abrupt change in Loop Current flow occurred at the top of MSC2, as a new erosional disconformity formed (Horizon H6, which dates to the Mid Pleistocene Transition; Hübscher and Nürnberg, 2023), marking the base of MSC3. This unit marks a return to contourite deposition characterized by large erosional moats on the up dip end of the eastern Campeche Bank. As there is no appreciable change in the slope of the Campeche Bank at this time, the mechanism for this change must be an increase in current velocity.

Hübscher and Nürnberg (2023) interpret the unit above the erosional disconformity at the MPT (our H6) as evidence of weakening of the Loop Current, but, given the lack of any equivalent sized moats in the underlying MSC2, we interpret the presence of moats in MSC3 as evidence of strengthening of the Loop Current. Hübscher and Nürnberg (2023) based their interpretations on the observation that offlapping reflectors below the MPT unconformity transition to onlapping reflectors above the MPT unconformity, indicating a deeper base level of current flow interacting with the seafloor below the unconformity and a shallower base level of current interaction above the unconformity. However, a transition from plastered drifts below the unconformity to elongated mounded drifts above, as is evident in our multichannel seismic data, indicates an increase in current velocity (e.g., Rebesco et al., 2014). The presence of the unconformity itself indicates that, for some period of time, current velocity increased to a point that the seafloor was primarily erosive and, to be sure, the resumption of deposition above this unconformity indicates a reduction in current velocity from that which caused the erosion, in agreement with Hübscher and Nürnberg (2023). Core data across this transition would help determine which of these hypotheses is correct.

5.2 Timing of Loop Current Development

No cores in or near our study area penetrate Horizon H4, which marks the base of seismic facies indicative of contourite drift deposition, and so we cannot be sure of the age of this unit. However, based on nearby cores and overall seismic facies we can develop a strong hypothesis.

DSDP Site 95 sits outside our study area on the edge of the Campeche Escarpment (Figure 1B). Site 95 cores show the overall stratigraphy of these deposits: a thin layer of Late Cretaceous strata unconformably overlain by a thick Paleogene section, which is unconformably overlain by Pleistocene ooze (Figure 10; Worzel et al, 1971). In those days, the *Glomar Challenger* would deploy a streamer and airguns and conduct its own site survey prior to drilling, and according to the seismic data published in the Initial Report for Leg 10 (Figure 10), at Site 95 Eocene and older high amplitude reflectors are overlain by Oligocene and Pleistocene low amplitude reflectors (Worzel et al., 1973). This change in seismic facies from high amplitude to low amplitude matches the shift observed in our seismic profiles between MSB3 (pre-drift) and MSC (contourite drift) (e.g., Figure 5, Figure 8). The Leg 10 shipboard scientists noted that this change in seismic character corresponds with the early Oligocene shift from chalk and cherty chalk to ooze (Worzel et al., 1973). Chert is known to occur in the Eocene across the Gulf of Mexico (e.g., Buffler et al., 1982) and well beyond (Muttoni and Kent, 2007). The physical characteristics (presence of chert, degree of lithification) of contemporaneous sediments are unlikely to change much over such a small area as the eastern Campeche Bank. We therefore think it is likely that the transition in seismic facies from high amplitude reflectors in MSB to low amplitude reflectors in MSC represents the sedimentological change from Eocene chalk and chert to Oligocene ooze. We thus interpret the onset of Loop Current to date back to around the Eocene-Oligocene Transition (Figure 10).

A small increase in grainsize of sortable silt at the Eocene to Oligocene at Site 95 indicates an increase in bottom water current velocity across the Eocene-Oligocene Transition (Figure 10). At more than 1800 m below modern sea level this increase in current velocity is more likely driven by an increase in intermediate or deep water moving into the basin than the Loop Current, but it is still evidence of invigorated current flow across this major climate transition. The Eocene-Oligocene Transition is associated with a strengthening of AMOC (Cramer et al., 2009; Hohbein et al., 2012; Borrelli et al.,2014; Abelson and Erez, 2017; Boyle et al., 2017; Coxall et al., 2018;

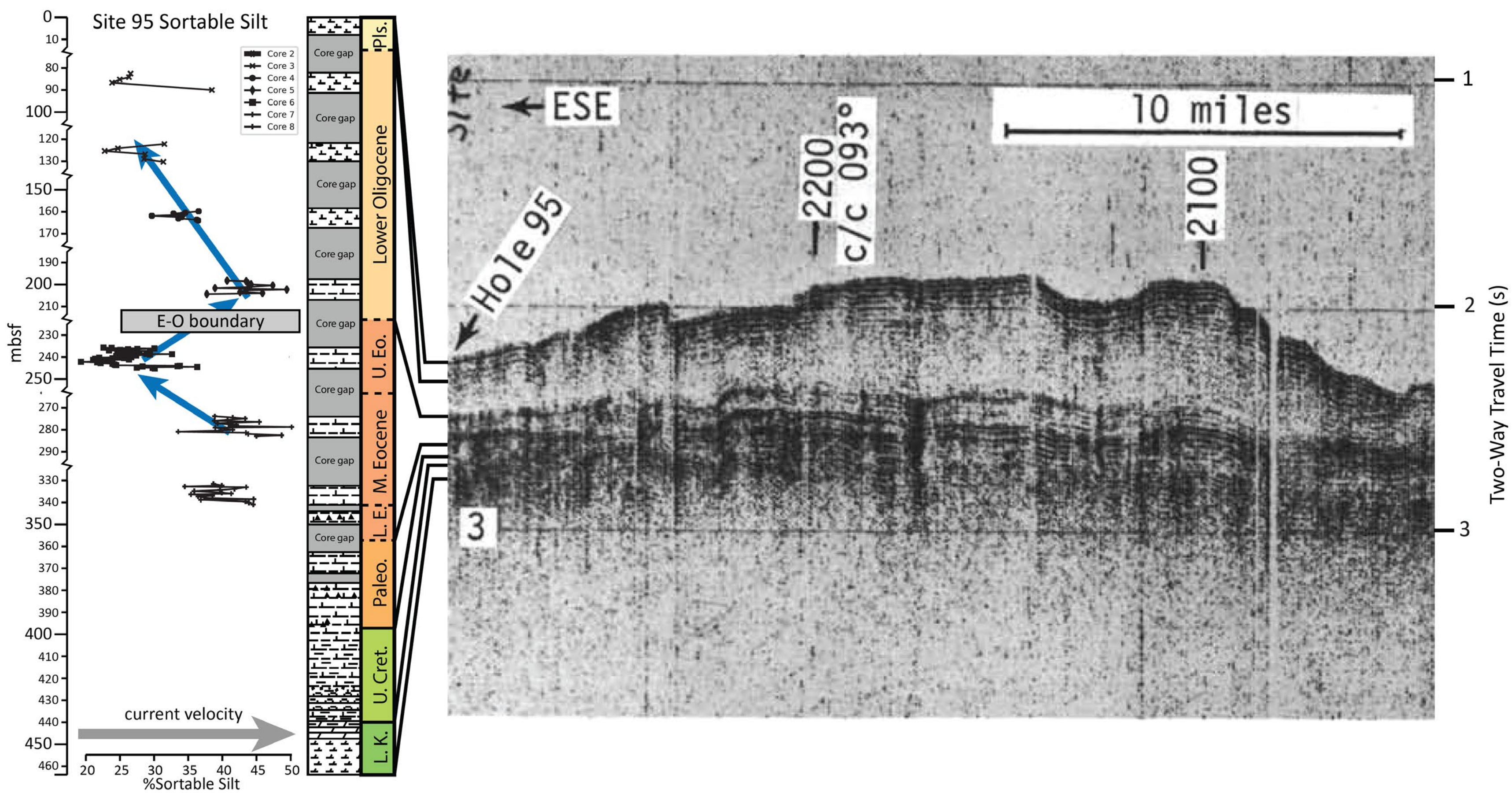

Figure 10. Stratigraphic column of DSDP Site 95 (after Worzel et al., 1971), sortable silt from DSDP Site 95, and the original seismic profile from the Glomar Challenger with ages from the core, cropped from Worzel et al. (1971). Note discontinuous depth scale on the stratigraphic column, necessary to see detail of grain size data. Site 95 was spot cored in the Cenozoic, a common practice in the early days of DSDP. See location map in Figure 1B.

Hutchinson et al., 2019), of which the Atlantic western boundary current system, including the Loop Current, is a key component.

Together, these observations all indicate that the Loop Current, in something like its present strength, began in response to the global cooling and strengthening overturning circulation at the Eocene-Oligocene Transition. This is the hypothesis we prefer because it matches the timing of the change in seismic facies at the closest core to the Campeche Bank drifts.

Alternatively, we can extrapolate from the sedimentation rate of 3.5 cm/kyr observed in the cores taken by Hübscher and Nürnberg (2019) and apply that rate to the full thickness of the observed sediment drifts. This requires making some assumptions. First, we must assume that sedimentation rate is constant. This is unlikely: the drifts themselves vary in thickness substantially, from about 200 m to about 500 m thick. Moreover, that thickness is not evenly distributed, so that MSC1 is thicker further updip than MSC2, which means that either sedimentation rate or erosion varies significantly across these deposits. We must also assume that the erosional disconformities don't represent much missing time. Recognizing all those caveats, we find that with a sedimentation rate of 3.5 cm/kyr with no hiatuses, a 500 m thick deposit (i.e., the maximum thickness of the MSC, which presumably would minimize any hiatuses) should date back to 14.3 Ma, the Middle Miocene.

The Middle Miocene is of course the generally accepted age for the development of the Loop Current and is coeval with the onset of drift deposition in the Santaren Channel in the Bahamas (12.4 Ma; Anselmetti et al., 2000) and Gardulski's (2001) estimate for the onset of drift current flow across the western Florida Platform. However, this age does not match the seismic facies or the chronostratigraphy of the nearest core to our study area, DSDP Site 95. The transition from high amplitude reflectors to low amplitude reflectors observed at Site 95 occurs at the Eocene-Oligocene Transition; within our study area it occurs at the transition from Megasequence B to Megasequence C (i.e., pre-drift to drift deposits). It is certainly possible that there is a significant hiatus between those two units and Pliocene or Miocene sediments are deposited on top of Eocene sediments, but we do not think that is likely, especially because Miocene and Pliocene sediments both appear to be entirely absent at Site 95 (Worzel et al., 1973).

Whatever the actual age of the base of MSC1, it seems clear that it must be older than the mid Pliocene, and that the Loop Current, in something close to its current form, predates the closure of the Central American Seaway and was instead initiated by some climatic shift in the mid to late Cenozoic. A planned coring expedition to the Campeche Bank will answer these questions more firmly.

6. Conclusions

Our high resolution multichannel seismic profiles of the Campeche Bank record the overall evolution of sedimentation and current flow at the southern aperture of the Gulf of Mexico. Megasequence A corresponds to Early Cretaceous platform carbonates. Megasequence B corresponds to Late Cretaceous and early Cenozoic pelagic carbonates, bisected by the high amplitude event layer associated with the Chicxulub Impact. Megasequence C corresponds to contourite current deposition and records the inception and evolution of the Loop Current. Megasequence C1 records the Loop Currents inception, with extensive erosion across the entire Campeche Bank and seismic facies indicative of elongated mounded drift deposits. Megasequence C2 records the transition to plastered drift deposits resulting from a shallowing slope as current flow reshaped the sediments on the Campeche Bank, and Megasequence C3 records the transition back to giant elongated mounded drift deposits in the Late Pleistocene.

With the exception of the short Pleistocene core in MSC3 reported by Hübscher and Nürnberg (2023), the lack of cores within our study area means that we cannot say with certainty when the Loop Current began. However, comparison to legacy seismic data across DSDP Site 95 reveals that the regional seismic facies shift from high amplitude reflectors to low amplitude reflectors, which corresponds to the base of contourite deposits in our study area, dates the Loop Current inception to the Eocene-Oligocene Transition. This indicates that the Loop Current developed during the global reorganization of ocean circulation that accompanied the first permanent southern hemisphere ice sheets. In the context of modern climate change, this is a comforting observation, as it means that while a climatic tipping point for the Loop Current likely exists, humanity is unlikely to cross that tipping point in any but the most extreme emissions scenarios.

However, it should be emphasized that a comparison of seismic facies in our modern high resolution seismic survey with seismic facies from low resolution (photocopied from the shipboard readout; Figure 10) seismic data from 1971 is not precise, and the Loop Current may be younger than the Oligocene. An alternate hypothesis, extrapolating from the sedimentation rate observed by Hübscher and Nürnberg (2023) in their Pleistocene core, suggests that the base of Megasequence C (and thus the Loop Current) dates to the Middle Miocene. This is in line with the commonly cited age of the development of the Loop Current, based on the onset of contourite drifts observed in the Florida Straits and the Santaren Channel in the Bahamas (Anselmetti et al., 2000; Paulat et al., 2019) and an invigoration of current flow across the western Florida Shelf (Gardulski et al., 1991). This has historically been assumed to have been driven by the closure of the Central American Seaway, but more recent results suggest that the final formation of the Isthmus of Panama, which blocked surface flow to the Pacific and redirected it north, did not occur until the mid Pliocene (O'Dea et al., 2016). If that tectonic gateway closure did not initiate the Loop Current, the most likely candidate is the climatic and oceanographic shift at the Middle Miocene Climate Transition, which drove a strengthening of North Atlantic Deep Water Formation (Knutz, 2008; Boyle et al., 2017). The Loop Current, like downwelling NADW, is part of AMOC, and increased downwelling means increased northward surface flow to compensate (e.g., Candela et al., 2019). In the context of modern climate change, a Middle Miocene inception of the Loop Current is particularly worrying, because we are very close to Middle Miocene pCO_2 values today (e.g., Steinthorsdottir et al., 2021). This would imply that we are also very close to a threshold at which the Loop Current could revert back to an earlier, weaker state. This reduction in the northward transport of warm, salty water would weaken NADW formation and profoundly alter Gulf of Mexico hydrography.

While we prefer an older, Oligocene age for Loop Current inception, neither hypothesis can be disproven without new core material from the Campeche Bank sediment drifts. Further work on this problem is imperative.

Acknowledgements

This work was supported by NSF-OCE-1928888, CONTEX 2018-38A, and a Pre-Drilling Activity Award from the U.S. Science Support Program (NSF prime award OCE-1450528). We are grateful for the patience and support of those programs and their program officers – Debbie Smith, Paloma Perry, and Angela Slagle – for supporting those grants through the disruptions of a global pandemic. We thank the Yucatán government for their support of this collaborative project. We also gratefully acknowledge the hard work of Lee Ellett, Kolby Pedrie, Brendon Mendenhall, Nick Benz, and Doug Penny in shipping, setting up, running, and troubleshooting the seismic equipment, Captain David Calles-Castillo and the crew of the *R/V Justo Sierra*, Holly Smith for coordinating NMFS permitting, our Protected Species Observers Yessica Vicencio, Yesenia Balderas, and Elsy Olivares, and Marcy Davis for her help processing multibeam data in conducting grain size analysis on DSDP Site 95 core material. We also thank Christian Hübscher for discussions at early planning stages of this study, and for sharing his interesting work as it was finished.

Conflict of Interest Statement

The authors are not aware of any affiliations or funding sources which may represent a conflict of interest with this work.

Data Availability Statement

Large format interpreted and uninterpreted seismic profiles are presented as supplemental material. Processed seismic data in SEG-Y format [will be, upon article acceptance] available from the Marine Geoscience Data System's Academic Seismic Portal [link].

Figure Captions

Figure 1. A) Regional surface currents associated with the North Atlantic western boundary current, including key oceanic gateways and passages for leakage of Northern Equatorial Current (N.E.C.) and Antilles Current waters into the Caribbean. B) Location map of the eastern Campeche Bank and surrounding waters, showing the location of our seismic survey, DSDP Site 95, and the mooring stations used to construct the vertical velocity profile reported in Candela et al. (2019)

(Figure 2). Basemap is the Global Multi-Resolution Topography dataset (Ryan et al., 2009) plotted in GeoMapApp(www.geomapapp.org) / CC BY.

Figure 2. Southeastern Gulf of Mexico hydrography. A) Temperature (T)/Salinity (S) and Temperature/Oxygen (O_2) for Yucatán Channel from Rivas et al. (2005) showing the watermasses that enter the Gulf through this aperture; SUW: Subtropical Underwater; 18W: 18 Sargasso Sea Water; TACW: Tropical Atlantic Central Water; AAIW: Antarctic Intermediate Water; NADW: North Atlantic Deep Water. B) Generalized schematic of circulation through the Gulf of Mexico, modified from Rivas et al. (2005). C) Mean current velocity in cm/s through the Yucatán Channel from September 2012 to August 2016 from Candela et al. (2019). Red contours represent northward flow and green contours southward counterflow; see Figure 1 for mooring locations.

Figure 3. Seismic facies, seismic units, and key horizons identified in our seismic survey. See text for description of seismic megasequences and sequence sets. Figure design inspired by Boyle et al. (2017).

Figure 4. Interpreted seismic profile of Line 1009, on the northern end of our study area. This profile shows relatively thinner drift deposits of MSC2, while MSC1 is limited to just the most up dip area, and MSC3 is not identified. A) multibeam bathymetry of active contourite moat in western end of profile; B) inset interpreted seismic profile showing development of reef margins in MSA (note thickening of Cretaceous pelagic sediments down dip of these margins); C) interpreted seismic profile; D) line drawing of interpreted profile. MTC: Mass Transport Complex. See location map in Figure 1B.

Figure 5. Interpreted seismic profile of Line 1005, which is notable for the dramatic incision of MSC1 into MSB, and for the large amalgamated channels in MSC1. (see inset). A) multibeam sonar bathymetry of sediment waves near western end of profile; B) inset interpreted seismic profile of notable erosional features in MSC1; C) interpreted seismic profile; D) line drawing of interpreted profile. See location map in Figure 1B.

Figure 6. Interpreted seismic profile of Line 1004, on the far southern end of our study area. The Campeche Bank drift is narrower here and mostly limited to the far western area of this profile,

updip of a steep early Cretaceous reef margin. Note thick K/Pg mass transport deposit at the foot of this relict escarpment. A deeper water drift complex, unrelated to the Loop Current, can be seen on the eastern end of this profile. A) interpreted seismic profile; B) line drawing of interpreted profile. See location map in Figure 1B.

Figure 7. Interpreted seismic profile of Line 1006, in the central part of our study area. The Campeche Bank drift is thick but contains fewer channels than nearby Line 1005. A) An amalgamated channel complex is present at the far updip end of MSC1; B) characteristic K/Pg boundary deposit with thicker deposit with fairly thick (~100 m) build up in a paleo low; C) interpreted seismic profile; D) line drawing of interpreted seismic profile. See location map in Figure 1B.

Figure 8. Interpreted seismic profile of Line 1003, the updip strike line. Northward dipping reflectors downlapping on Horizon H5 show deposition across the entire length of the contourite drift. Extensive erosion along Horizon H4 (representing the base of contourite drift deposition) is occurs across the entire profile and is particularly evident at the far northern and southern ends. A) An amalgamated channel complex is present at the far updip end of MSC1; B) characteristic K/Pg boundary deposit with thicker deposit with fairly thick (~100 m) build up in a paleo low; C) interpreted seismic profile; D) line drawing of interpreted seismic profile. See location map in Figure 1B.

Figure 9. Interpreted seismic profile of Line 1001, the downdip strike line. Of particular interest in this line is the erosional escarpment on the southern end, facing the Campeche Channel. Even below 1000 m there appears to be active erosion at the seafloor. A) interpreted seismic profile; B) line drawing of interpreted seismic profile.

Figure 10. Stratigraphic column of DSDP Site 95 (after Worzel et al., 1971), sortable silt from DSDP Site 95, and the original seismic profile from the Glomar Challenger with ages from the core, cropped from Worzel et al. (1971). Note discontinuous depth scale on the stratigraphic column, necessary to see detail of grain size data. Site 95 was spot cored in the Cenozoic, a common practice in the early days of DSDP. See location map in Figure 1B.

References

Abelson, M., & Erez, J. (2017). The onset of modern-like Atlantic meridional overturning circulation at the Eocene-Oligocene transition: Evidence, causes, and possible implications for global cooling. *Geochemistry, Geophysics, Geosystems*, *18*(6), 2177-2199.

Abascal, A. J., Sheinbaum, J., Candela, J., Ochoa, J., & Badan, A. (2003). Analysis of flow variability in the Yucatan Channel. *Journal of Geophysical Research: Oceans*, *108*(C12).

Androulidakis, Y., Kourafalou, V., Olascoaga, M. J., Beron-Vera, F. J., Le Hénaff, M., Kang, H., & Ntaganou, N. (2021). Impact of Caribbean anticyclones on Loop Current variability. *Ocean dynamics*, 71(9), 935-956.

Angstadt, D. M., Austin Jr, J. A., & Buffler, R. T. (1985). Early Late Cretaceous to Holocene seismic stratigraphy and geologic history of southeastern Gulf of Mexico. *AAPG Bulletin*, *69*(6), 977-995.

Antoine, J. W., Martin Jr, R. G., Pyle, T. G., & Bryant, W. R. (1974). Continental margins of the Gulf of Mexico. In *The geology of continental margins* (pp. 683-693). Berlin, Heidelberg: Springer Berlin Heidelberg.

Anselmetti, F. S., Eberli, G. P., & Ding, Z. D. (2000). From the Great Bahama Bank into the Straits of Florida: a margin architecture controlled by sea-level fluctuations and ocean currents. *Geological Society of America Bulletin*, *112*(6), 829-844.

Arellano-Torres, E., Amezcua-Montiel, A., & Casas-Ortiz, A. (2023). The Loop Current circulation over the MIS 9 to MIS 5 based on planktonic foraminifera assemblages from the Gulf of Mexico. *Paleoceanography and Paleoclimatology*, e2022PA004568.

Austin Jr, J. A., Schlager, W., & Palmer, A. A. (1986). Leg 101. *Proceedings initial reports (Pt. A). Ocean Drilling Program, College Station, TX*.

Badan Jr, A., Candela, J., Sheinbaum, J., & Ochoa, J. (2005). Upper-layer circulation in the approaches to Yucatan Channel. *Washington DC American Geophysical Union Geophysical Monograph Series*, *161*, 57-69.

Biggs, D. C. (1992). Nutrients, plankton, and productivity in a warm-core ring in the western Gulf of Mexico. *Journal of Geophysical Research: Oceans*, *97*(C2), 2143-2154.

Borrelli, C., Cramer, B. S., & Katz, M. E. (2014). Bipolar Atlantic deepwater circulation in the middle-late Eocene: Effects of Southern Ocean gateway openings. *Paleoceanography*, *29*(4), 308-327.

Bosart, L. F., Bracken, W. E., Molinari, J., Velden, C. S., & Black, P. G. (2000). Environmental influences on the rapid intensification of Hurricane Opal (1995) over the Gulf of Mexico. *Monthly Weather Review*, *128*(2), 322-352.

Boyle, P. R., Romans, B. W., Tucholke, B. E., Norris, R. D., Swift, S. A., & Sexton, P. F. (2017). Cenozoic North Atlantic deep circulation history recorded in contourite drifts, offshore Newfoundland, Canada. *Marine Geology*, *385*, 185-203.

Bralower, T. J., Paull, C. K., & Mark Leckie, R. (1998). The Cretaceous-Tertiary boundary cocktail: Chicxulub impact triggers margin collapse and extensive sediment gravity flows. *Geology*, *26*(4), 331-334.

Brunner, C. A. (1984). Evidence for increased volume transport of the Florida Current in the Pliocene and Pleistocene. *Marine Geology*, *54*(3-4), 223-235.

Buffler, R. T., J. S. Watkins, F. J. Schaub, and J. L. Worzel, 1980, Structure and early geologic history of the deep central Gulf of Mexico basin, *in* R. H. Pilger, ed., The origin of the Gulf of Mexico and the early opening of the central North Atlantic Ocean, a symposium: Baton Rouge, Louisiana State University, p. 3-16.

Buffler, R.T., Schlager, W., et al. (1984), Initial reports of Deep Sea Drilling Project, *v,* 77, 747 p.

Burg, J.P. (1975) *Maximum entropy spectral analysis*. Stanford University

Candela, J., Sheinbaum, J., Ochoa, J., Badan, A., & Leben, R. (2002). The potential vorticity flux through the Yucatan Channel and the Loop Current in the Gulf of Mexico. *Geophysical Research Letters*, *29*(22), 16-1.

Candela, J., Tanahara, S., Crepon, M., Barnier, B., & Sheinbaum, J. (2003). Yucatan Channel flow: Observations versus CLIPPER ATL6 and MERCATOR PAM models. *Journal of Geophysical Research: Oceans*, *108*(C12).

Candela, J., Ochoa, J., Sheinbaum, J., Lopez, M., Perez-Brunius, P., Tenreiro, M., Pallàs-Sanz, E. Athié, G., & Arriaza-Oliveros, L. (2019). The flow through the gulf of Mexico. *Journal of Physical Oceanography*, *49*(6), 1381-1401.

Chang, Y. L., & Oey, L. Y. (2012). Why does the Loop Current tend to shed more eddies in summer and winter?. *Geophysical Research Letters*, *39*(5).

Chen, C. S., 1965, The regional lithostratigraphic analysis of Paleocene andEocene rocks of Florida: Florida Geological Survey Bulletin, v. 45, I05 p.

Coxall, H. K., Huck, C. E., Huber, M., Lear, C. H., Legarda-Lisarri, A., O'regan, M., Sliwinksa, K. K., Van De Flierdt, T., De Boer, A. M., Zachos, J. C., & Backman, J. (2018). Export of nutrient rich Northern Component Water preceded early Oligocene Antarctic glaciation. *Nature Geoscience*, *11*(3), 190-196.

Cramer, B. S., Toggweiler, J. R., Wright, J. D., Katz, M. E., & Miller, K. G. (2009). Ocean overturning since the Late Cretaceous: Inferences from a new benthic foraminiferal isotope compilation. *Paleoceanography*, *24*(4).

Denne, R. A., Scott, E. D., Eickhoff, D. P., Kaiser, J. S., Hill, R. J., & Spaw, J. M. (2013). Massive Cretaceous-Paleogene boundary deposit, deep-water Gulf of Mexico: New evidence for widespread Chicxulub-induced slope failure. *Geology*, *41*(9), 983-986.

Denny III, W. M., Austin, J. A., & Buffler, R. T. (1994). Seismic stratigraphy and geologic history of middle Cretaceous through Cenozoic rocks, southern Straits of Florida. *AAPG bulletin*, *78*(3), 461-487.

Droxler, A. W., Burke, K. C., Cunningham, A. D., Hine, A. C., Rosencrantz, E., Duncan, D. S., Hallock, P., & Robinson, E. (1998). Caribbean constraints on circulation between Atlantic and Pacific Oceans over the past 40 million years.

Faugères, J. C., Stow, D. A., Imbert, P., & Viana, A. (1999). Seismic features diagnostic of contourite drifts. *Marine Geology*, *162*(1), 1-38.

Gardulski, A. F., Gowen, M. H., Milsark, A., Weiterman, S. D., Wise Jr, S. W., & Mullins, H. T. (1991). Evolution of a deep-water carbonate platform: Upper Cretaceous to Pleistocene sedimentary environments on the west Florida margin. *Marine Geology*, *101*(1-4), 163-179.

Hildebrand, A. R., Penfield, G. T., Kring, D. A., Pilkington, M., Camargo Z, A., Jacobsen, S. B., & Boynton, W. V. (1991). Chicxulub crater: a possible Cretaceous/Tertiary boundary impact crater on the Yucatan Peninsula, Mexico. *Geology*, *19*(9), 867-871.

Hine, A.C. (2013) Geologic History of Florida—Major Events That Formed the Sunshine State. University Press of Florida, Gainesville, FL, 256 pp.

Hohbein, M. W., Sexton, P. F., & Cartwright, J. A. (2012). Onset of North Atlantic Deep Water production coincident with inception of the Cenozoic global cooling trend. *Geology*, *40*(3), 255-258.

Holbourn, A., Kuhnt, W., Kochhann, K. G., Matsuzaki, K. M., & Andersen, N. (2022). Middle Miocene climate–carbon cycle dynamics: Keys for understanding future trends on a warmer Earth?.

Hübscher, C., Dullo, C., Flögel, S., Titschack, J., & Schönfeld, J. (2010). Contourite drift evolution and related coral growth in the eastern Gulf of Mexico and its gateways. *International Journal of Earth Sciences*, *99*, 191-206.

Hübscher, C., & Nürnberg, D. (2023). Loop Current attenuation after the Mid-Pleistocene Transition contributes to Northern hemisphere cooling. *Marine Geology*, *456*, 106976.

Hübscher, C., Häcker, T., Betzler, C., Kalvelage, C., & Weiß, B. (2023). Reading the sediment archive of the Eastern Campeche Bank (southern Gulf of Mexico): from the aftermath of the Chicxulub impact to Loop Current variability. *Marine Geophysical Research*, *44*(2), 6.

Hutchinson, D. K., Coxall, H. K., O′Regan, M., Nilsson, J., Caballero, R., & de Boer, A. M. (2019). Arctic closure as a trigger for Atlantic overturning at the Eocene-Oligocene Transition. *Nature Communications*, *10*(1), 3797.

Jaimes, B., & Shay, L. K. (2009). Mixed layer cooling in mesoscale oceanic eddies during Hurricanes Katrina and Rita. *Monthly Weather Review*, *137*(12), 4188-4207.

Jaimes, B., Shay, L. K., & Brewster, J. K. (2016). Observed air-sea interactions in tropical cyclone Isaac over Loop Current mesoscale eddy features. *Dynamics of Atmospheres and Oceans*, *76*, 306-324.

Kameo, K., & Sato, T. (2000). Biogeography of Neogene calcareous nannofossils in the Caribbean and the eastern equatorial Pacific—floral response to the emergence of the Isthmus of Panama. *Marine Micropaleontology*, *39*(1-4), 201-218.

Knutz, P. C. (2008). Palaeoceanographic significance of contourite drifts. *Developments in sedimentology*, *60*, 511-535.

Lindo-Atichati, D., Bringas, F., Goni, G., Muhling, B., Muller-Karger, F. E., & Habtes, S. (2012). Varying mesoscale structures influence larval fish distribution in the northern Gulf of Mexico. *Marine Ecology Progress Series*, *463*, 245-257.

Livermore, R., Hillenbrand, C. D., Meredith, M., & Eagles, G. (2007). Drake Passage and Cenozoic climate: an open and shut case?. *Geochemistry, Geophysics, Geosystems*, *8*(1).

Lowery, C. M., & Bralower, T. J. (2022). Elevated Post K-Pg Export Productivity in the Gulf of Mexico and Caribbean. *Paleoceanography and Paleoclimatology*, *37*(9), e2021PA004400.

Marton, G. L., & Buffler, R. T. (1999). Jurassic—Early Cretaceous tectono-paleogeographic evolution of the southeastern Gulf of Mexico basin. In *Sedimentary basins of the world* (Vol. 4, pp. 63-91). Elsevier.

McCave, I. N., Thornalley, D. J. R., & Hall, I. R. (2017). Relation of sortable silt grain-size to deep-sea current speeds: Calibration of the 'Mud Current Meter'. *Deep Sea Research Part I: Oceanographic Research Papers*, *127*, 1-12.

Milkov, A. V., & Sassen, R. (2000). Thickness of the gas hydrate stability zone, Gulf of Mexico continental slope. *Marine and petroleum Geology*, *17*(9), 981-991.

Mullins, H. T., Gardulski, A. F., WISE Jr, S. W., & Applegate, J. (1987). Middle Miocene oceanographic event in the eastern Gulf of Mexico: implications for seismic stratigraphic succession and Loop Current/Gulf Stream circulation. *Geological Society of America Bulletin*, *98*(6), 702-713.

Mutti, M., Droxler, A. W., & Cunningham, A. D. (2005). Evolution of the Northern Nicaragua Rise during the Oligocene–Miocene: drowning by environmental factors. *Sedimentary Geology*, *175*(1-4), 237-258.

Muttoni, G., & Kent, D. V. (2007). Widespread formation of cherts during the early Eocene climate optimum. *Palaeogeography, Palaeoclimatology, Palaeoecology*, *253*(3-4), 348-362.

National Academies of Sciences, Engineering, and Medicine. 2018. Understanding and Predicting the Gulf of Mexico Loop Current: Critical Gaps and Recommendations. Washington, DC: The National Academies Press. https://doi.org/10.17226/24823.

Nielsen, T. A. P. M., Knutz, P. C., & Kuijpers, A. (2008). Seismic expression of contourite depositional systems. *Developments in Sedimentology*, *60*, 301-321.

Ochoa, J., Badan, A., Sheinbaum, J., & Candela, J. (2003). CANEK: Measuring transport in the Yucatan Channel. *Nonlinear Processes in Geophysical Fluid Dynamics. Kluwer Academic Publishers, Dordrecht*, 275-286.

O'Dea, A., Lessios, H. A., Coates, A. G., Eytan, R. I., Restrepo-Moreno, S. A., Cione, A. L., Collins, L. S., De Quieroz, A., Farris, D. W., Norris, R. D., Stallard, R. F., Woodburne, M. O., Aguilera, O., Aubry, M.-P., Berggren, W. P., Budd, A. F., Cozzuol, M. A., Coppard, S. E., Duque-Caro, H., Finnegan, S., Gasparini, G. M., Grossman, E. L., Johnson, K. G., Keigwin, L. D., Knowlton, N., Leigh, E. G., Leonard-Pingel, J. S., Vermeij, G., & Jackson, J. B. (2016). Formation of the Isthmus of Panama. *Science advances*, *2*(8), e1600883.

Paulat, M., Lüdmann, T., Betzler, C., & Eberli, G. P. (2019). Neogene palaeoceanographic changes recorded in a carbonate contourite drift (Santaren Channel, Bahamas). *Sedimentology*, *66*(4), 1361-1385.

Pindell, J. L., & Kennan, L. (2009). Tectonic evolution of the Gulf of Mexico, Caribbean and northern South America in the mantle reference frame: an update. *Geological Society, London, Special Publications*, *328*(1), 1-55.

Pinet, P. R., & Popenoe, P. (1985). A scenario of Mesozoic-Cenozoic ocean circulation over the Blake Plateau and its environs. *Geological Society of America Bulletin*, *96*(5), 618-626.

Poore, R. Z., Quinn, T. M., & Verardo, S. (2004). Century-scale movement of the Atlantic Intertropical Convergence Zone linked to solar variability. *Geophysical Research Letters*, *31*(12).

Popenoe, P., Henry, V. J., & Idris, F. M. (1987). Gulf trough—the Atlantic connection. *Geology*, *15*(4), 327-332.

Potter, H., DiMarco, S. F., & Knap, A. H. (2019). Tropical cyclone heat potential and the rapid intensification of Hurricane Harvey in the Texas Bight. *Journal of Geophysical Research: Oceans*, *124*(4), 2440-2451.

Rebesco, M., Hernández-Molina, F. J., Van Rooij, D., & Wåhlin, A. (2014). Contourites and associated sediments controlled by deep-water circulation processes: State-of-the-art and future considerations. *Marine Geology*, *352*, 111-154.

Rivas, D., Badan, A., & Ochoa, J. (2005). The ventilation of the deep Gulf of Mexico. *Journal of physical oceanography*, *35*(10), 1763-1781.

Roth, J. M., Droxler, A. W., & Kameo, K. (2000). THE CARIBBEAN CARBONATE CRASH AT THE MIDDLE TO LATE MIOCENE TRANSITION: LINKAGE TO THE ESTABLISHMENT OF THE MODERN GLOBAL OCEAN CONVEYOR. *in* Leckie, R.M., Sigurdsson, H., Acton, G.D., and Draper, G. (Eds.), *Proceedings of the Ocean Drilling Program, Scientific Results*, Vol. 165

Rousset, C., & Beal, L. M. (2011). On the seasonal variability of the currents in the Straits of Florida and Yucatan Channel. *Journal of Geophysical Research: Oceans*, *116*(C8).

Ryan, W. B. F., S.M. Carbotte, J. Coplan, S. O'Hara, A. Melkonian, R. Arko, R.A. Weissel, V. Ferrini, A. Goodwillie, F. Nitsche, J. Bonczkowski, and R. Zemsky (2009), Global Multi-Resolution Topography (GMRT) synthesis data set, Geochem. Geophys. Geosyst., 10, Q03014, doi:10.1029/2008GC002332.

Sanford, J. C., Snedden, J. W., & Gulick, S. P. (2016). The Cretaceous-Paleogene boundary deposit in the Gulf of Mexico: Large-scale oceanic basin response to the Chicxulub impact. *Journal of Geophysical Research: Solid Earth*, *121*(3), 1240-1261.

Shaub, F.J. (1983). Origin of Catoche Tongue, *In* Bally, A.W., *A Picture and Work Atlas. Seismic Expressions of Structural Styles*, Vol. 2 (2.2.3-129 -2.2.2-139). *American Association of Petroleum Geologists. Studies in Geology Series # 15.*

Schmitz Jr, W. J., & McCartney, M. S. (1993). On the north Atlantic circulation. *Reviews of Geophysics*, *31*(1), 29-49.

Sickmann, Z. T., & Snedden, J. W. (2020). Neogene to recent evolution of the Southern Gulf of Mexico basin: Tectonic controls on deep-water sediment dispersal systems. *Basin Research*, *33*(2), 1240-1265.

Snedden, J. W., & Galloway, W. E. (2019). *The Gulf of Mexico sedimentary basin: Depositional evolution and petroleum applications*. Cambridge University Press.

Sohl, N. F., Martínez, E. R., Salmerón-Ureña, P., Soto-Jaramillo, F., & Salvador, A. (1991). The Gulf of Mexico Basin. *Boulder, Colorado, Geological Society of America, Geology of North America*, 205-244.

Steinberg, J. M., Piecuch, C. G., Hamlington, B. D., Thompson, P. R., & Coats, S. (2023). Influence of Deep-Ocean Warming on Coastal Sea-Level Trends in the Gulf of Mexico. *Authorea Preprints*.

Steinthorsdottir, M., Coxall, H. K., De Boer, A. M., Huber, M., Barbolini, N., Bradshaw, C. D., Burls, N. J., Feakins, S. J., Gasson, E., Hendriks, J., Holbourn, A. E., Kiel, S., Kohn, M. J., Kürschner, W. M., Lear, C. H., Liebrand, D., Lunt, D. J., Mörs, T., Pearson, P. N.,Pound, M. J., Stoll, H. & Strömberg, C. A. E. (2021). The Miocene: the future of the past. *Paleoceanography and Paleoclimatology*, *36*(4), e2020PA004037.

Sturges, W., & Leben, R. (2000). Frequency of ring separations from the Loop Current in the Gulf of Mexico: A revised estimate. *Journal of Physical Oceanography*, *30*(7), 1814-1819.

Ward, W. C., Keller, G., Stinnesbeck, W., & Adatte, T. (1995). Yucatán subsurface stratigraphy: Implications and constraints for the Chicxulub impact. *Geology*, *23*(10), 873-876.

Weisberg, R. H., & Liu, Y. (2017). On the Loop Current penetration into the Gulf of Mexico. *Journal of Geophysical Research: Oceans*, *122*(12), 9679-9694.

Worzel, J. L., Bryant, W., and Leg 10 Shipboard Scientists (1971). *Initial Reports of the Deep Sea Drilling Project*, 10, U.S. Government Printing Office, Washington, DC

Yilmaz, Ö. (2001). *Seismic data analysis: Processing, inversion, and interpretation of seismic data*. Society of Exploration Geophysicists.